

## Manifold learning with arbitrary norms

Joe Kileel\* · Amit Moscovich ·  
Nathan Zelesko · Amit Singer

**Abstract** Manifold learning methods play a prominent role in nonlinear dimensionality reduction and other tasks involving high-dimensional data sets with low intrinsic dimensionality. Many of these methods are graph-based: they associate a vertex with each data point and a weighted edge between each pair of close points. Existing theory shows, under certain conditions, that the Laplacian matrix of the constructed graph converges to the Laplace-Beltrami operator of the data manifold. However, this result assumes the Euclidean norm is used for measuring distances. In this paper, we determine the limiting differential operator for graph Laplacians constructed using *any* norm. The proof involves a subtle interplay between the second fundamental form of the underlying manifold and the convex geometry of the norm's unit ball. To motivate the use of non-Euclidean norms, we show in a numerical simulation that manifold learning based on Earthmover's distances outperforms the standard Euclidean variant for learning molecular shape spaces, in terms of both sample complexity and computational complexity.

**Keywords** dimensionality reduction · diffusion maps · Laplacian eigenmaps · second-order differential operator · Riemannian geometry · convex body

---

\*Author to whom correspondence should be addressed.

Joe Kileel  
Department of Mathematics and Oden Institute, University of Texas at Austin  
E-mail: jkileel@math.utexas.edu

Amit Moscovich  
Program in Applied and Computational Mathematics, Princeton University  
E-mail: amit@moscovich.org

Nathan Zelesko  
Department of Mathematics, Brown University  
E-mail: nathan@zelesko.com

Amit Singer  
Department of Mathematics and Program in Applied and Computational Mathematics,  
Princeton University  
E-mail: amits@math.princeton.edu

## 1 Introduction

*Manifold learning* is broadly concerned with analyzing high-dimensional data sets that have a low intrinsic dimensionality. This field includes unsupervised dimensionality reduction [4, 16, 11, 41], supervised and semi-supervised regression and classification on manifolds [5, 7, 28, 21, 63, 10, 37, 27, 46], signal processing on manifolds [24, 31, 20, 29] and the estimation of various geometric and topological quantities [19, 9, 59, 2, 26]. A standard assumption in manifold learning is that the input points lie on (or close to) a  $d$ -dimensional manifold  $\mathcal{M}$  that is a submanifold of  $\mathbb{R}^D$ ,

$$\mathbf{x}_1, \dots, \mathbf{x}_n \in \mathcal{M} \subseteq \mathbb{R}^D. \quad (1)$$

Many of the methods for manifold learning follow a graph-based paradigm. They first construct an undirected weighted graph, whose edge weights correspond to pairwise affinities, for example

$$W_{ij} = \exp(-\|\mathbf{x}_i - \mathbf{x}_j\|^2 / \sigma^2). \quad (2)$$

The resulting graph is then used as a proxy for the (typically unknown) manifold. For example, the basic idea behind the ISOMAP algorithm [54] is that geodesic distances on a suitably chosen affinity graph converge in probability to the manifold geodesic distances.

Some of the most popular graph-based methods for manifold learning are based on harmonic analysis. In analogy to classical Fourier analysis, one can perform signal estimation and processing using a basis of eigenfunctions of the Laplacian on a manifold. Two closely related methods for this are Laplacian eigenmaps [4] and diffusion maps [11]. Their key observation is that the manifold Laplacian (or Laplace-Beltrami operator) can be approximated by the Laplacian matrix of a weighted graph with edge weights given by Equation (2). The graph Laplacian eigenvectors can then be computed and used for data processing tasks in a manner that is analogous to the many applications of the Fourier basis [22, 32]. Current theory for graph Laplacian methods assumes that the pairwise affinities are based on the Euclidean (or  $\ell_2$ ) norm. However, depending on the domain of the data, other norms may be preferable.

### 1.1 Our contribution

The main contribution of this paper is a proof of the convergence of graph Laplacians based on arbitrary norms. In Theorem 1, we show that using *any* norm  $\|\cdot\|$ , graph Laplacians constructed with the Gaussian affinity enjoy pointwise-convergence to an explicit second-order differential operator on  $\mathcal{M}$ . Interestingly, unlike the case of the Euclidean norm, the limiting operator is not intrinsic to the manifold, i.e., it depends on the embedding of  $\mathcal{M}$  in  $\mathbb{R}^D$ . Furthermore, it has non-vanishing and possibly discontinuous first order terms.

In a second contribution, we present in Section 4 a variant of diffusion maps that is based on an approximate Earthmover’s distance (Wasserstein-1 metric)

for learning shape spaces with continuous variability. This is motivated by an important problem in structural biology: learning the conformation space of flexible proteins and other macromolecules with continuous variability from cryo-electron microscopy images [17]. Since the Earthmover’s distance is induced from a norm (see [56, Remark 1.15(ii)]), our theorem applies in this case.

## 1.2 Background: manifold learning based on the graph Laplacian

Given a data set  $V = \{\mathbf{x}_1, \dots, \mathbf{x}_n\}$  sampled from a normed space  $(\mathcal{X}, \|\cdot\|)$  and an affinity function  $K_\sigma : \mathbb{R}_{\geq 0} \rightarrow \mathbb{R}_{\geq 0}$ , consider the matrix of pairwise affinities:

$$W_{ij} := K_\sigma(\|\mathbf{x}_i - \mathbf{x}_j\|). \quad (3)$$

The canonical choice for  $K_\sigma$  is the Gaussian kernel,  $K_\sigma(t) = \exp(-t^2/\sigma^2)$  (up to normalization conventions). Another possibility is the 0/1 kernel,  $K_\sigma(t) = \mathbb{1}(t \leq \sigma)$ . The matrix  $W$  defines a weighted graph  $G = (V, E, W)$  where the set of edges  $E$  is comprised of all the pairs  $(i, j)$  for which  $W_{ij} > 0$ . Define the degree matrix by  $D_{ij} = \delta_{ij} \sum_k W_{ik}$ . The (unnormalized) negative semi-definite *graph Laplacian* is the matrix

$$\mathcal{L}_G := W - D. \quad (4)$$

The graph Laplacian acts on vectors  $f \in \mathbb{R}^n$  in the following way:

$$(\mathcal{L}_G f)_i = \sum_{j=1}^n w_{ij}(f_j - f_i). \quad (5)$$

$\mathcal{L}_G$  is a symmetric negative semi-definite matrix with eigenvalues

$$0 = \lambda_0 \geq \lambda_1 \geq \dots \geq \lambda_{n-1}. \quad (6)$$

Its eigenvectors  $\phi_0, \dots, \phi_n \in \mathbb{R}^n$  can be chosen to be real and orthonormal. The constant vector  $\phi_0 = n^{-1/2} \mathbf{1}$  is an eigenvector with eigenvalue zero. For more on the properties of the graph Laplacian and its normalized variants, see the tutorial by von Luxburg [58].

*Remark 1* Several other authors use the positive semi-definite graph Laplacian convention,  $\mathcal{L}_G^{\text{psd}} := D - W$ . However, in this paper, we chose the negative semi-definite convention for technical convenience.

The eigenvectors of the graph Laplacian are often viewed as real functions whose domain is the set of graph vertices,

$$\phi_i : V \rightarrow \mathbb{R}. \quad (7)$$

There are two common uses for the Laplacian eigenvectors:

1. As a basis for function representation and approximation [5, 12, 32],

$$g(\mathbf{x}_i) = \sum_j \alpha_j \phi_j(\mathbf{x}_i). \quad (8)$$

2. As a method for dimensionality reduction of the input set  $\mathbf{x}_1, \dots, \mathbf{x}_n$ . An  $m$ -dimensional embedding is given by mapping each data point according to the first  $m$  Laplacian eigenvectors [4, 11],

$$\mathbf{x}_i \mapsto (\phi_1(\mathbf{x}_i), \dots, \phi_m(\mathbf{x}_i)). \quad (9)$$

This is motivated by the fact that any closed connected Riemannian manifold is smoothly embedded into  $\mathbb{R}^m$  by its first  $m$  Laplacian eigenfunctions, for some choice of  $m$  [3].

### 1.3 Existing theory: graph Laplacians using the Euclidean norm

Let us assume that the input space is  $\mathbb{R}^D$ , equipped with the standard Euclidean norm  $\|\cdot\|_2$ . If the points  $\mathbf{x}_1, \dots, \mathbf{x}_n$  are sampled i.i.d. from a uniform probability distribution on a compact submanifold  $\mathcal{M} \subseteq \mathbb{R}^D$  then the graph Laplacian enjoys pointwise convergence to the manifold Laplacian, or Laplace-Beltrami operator (see [23, 51, 6]). For a non-uniform probability distribution, variants of the graph Laplacian converge to a weighted Laplacian, or Fokker-Planck operator, which has an additional density-dependent drift term (see [11, 47, 55]). In addition to pointwise consistency, spectral consistency was proved [39, 48, 18], i.e., the convergence of the graph Laplacian eigenvalues and eigenvectors to the eigenvalues and eigenfunctions of the limiting differential operator, where the convergence of the discrete eigenvectors to the continuous eigenfunctions is understood in an appropriate sense.

In all previous theoretical analyses, the norm used for forming the affinity matrix in Equation (3) is the standard Euclidean norm  $\|\cdot\|_2$ . It is worth stressing that the convergence proof for the Euclidean case is *not* directly adaptable to the case of other norms. In particular, it relies on a special property of the Euclidean norm: that Euclidean distances provide a second-order approximation to manifold geodesic distances (see [6, Figure 1]).

## 2 Ingredients and theorem statement

The goal of this section is to state our main result, Theorem 1: the pointwise convergence of graph Laplacians formed using an arbitrary norm to a certain continuous differential operator on the manifold. To this end, we first collect together the needed tools from differential geometry and a little convex geometry. These preliminaries set notation and keep this paper self-contained. Next, we emphasize the importance of Subsection 2.3: here we introduce a construction, which we name the *tilt construction*, that captures a certain second-order relationship between a manifold and the unit ball of a given norm. We will later prove that this tilt function corresponds to the first-order derivative term in the limiting differential operator. In Subsection 2.4, we state Theorem 1. Then we restate it a couple times to discuss useful reinterpretations. Finally, two examples are worked in Subsections 2.5 and 2.6 to illustrate Theorem 1.

## 2.1 Notation and preliminaries from Riemannian geometry

Here we review some basics from Riemannian geometry, and set notation. These are later used for our theorem statement and our proof. We point the reader to Lee's books [34, 35] for wonderful accounts of differential geometry.

Let  $\mathcal{M} \subseteq \mathbb{R}^D$  denote a  $d$ -dimensional compact smooth embedded *Riemannian manifold*. Let  $\mathbf{p} \in \mathcal{M}$  denote a point. We write  $T_{\mathbf{p}}\mathcal{M}$  for the (abstract) *tangent space* to  $\mathcal{M}$  at  $\mathbf{p}$  (see [35, Chapter 3]). In particular,  $T_{\mathbf{p}}\mathcal{M}$  is a  $d$ -dimensional real vector space equipped with an inner product  $\langle \cdot, \cdot \rangle_{\mathbf{p}}$ . Here,  $0 \in T_{\mathbf{p}}\mathcal{M}$  and we do not consider  $T_{\mathbf{p}}\mathcal{M}$  to be embedded in  $\mathbb{R}^D$ . The *exponential map* at  $\mathbf{p}$  [34, Chapter 5], denoted  $\exp_{\mathbf{p}} : T_{\mathbf{p}}\mathcal{M} \rightarrow \mathcal{M}$  is a map that carries straight lines in  $T_{\mathbf{p}}\mathcal{M}$  through 0 to *geodesics* on  $\mathcal{M}$  that go through  $\mathbf{p}$ .<sup>1</sup> By compactness of  $\mathcal{M}$ , the Hopf-Rinow theorem allows  $\exp_{\mathbf{p}}$  to be defined on the whole tangent space  $T_{\mathbf{p}}\mathcal{M}$ . One can fix open neighborhoods  $U \subseteq T_{\mathbf{p}}\mathcal{M}$  of 0 and  $V \subseteq \mathcal{M}$  of  $\mathbf{p}$  such that the exponential map restricts to a *diffeomorphism*,

$$\exp_{\mathbf{p}} : U \xrightarrow{\sim} V. \quad (10)$$

Further, let us fix an orthonormal basis on  $T_{\mathbf{p}}\mathcal{M}$  with respect to  $\langle \cdot, \cdot \rangle_{\mathbf{p}}$ , and write  $\mathbf{s} = (s_1, \dots, s_d)^\top$  for coordinates on  $U$  with respect to this basis; these are *geodesic normal coordinates* for  $\mathcal{M}$  around  $\mathbf{p}$  with (10) as the chart. By abusing notation, identify  $\exp_{\mathbf{p}}$  with  $\iota \circ \exp_{\mathbf{p}}$ , where  $\iota : \mathcal{M} \hookrightarrow \mathbb{R}^D$  is inclusion. Then  $\exp_{\mathbf{p}}$  is a smooth mapping from an open subset of Euclidean space  $\mathbb{R}^d$  into Euclidean space  $\mathbb{R}^D$ , and thus it admits a Taylor expansion around  $\mathbf{s} = 0$ :

$$\exp_{\mathbf{p}}(\mathbf{s}) = \mathbf{p} + L_{\mathbf{p}}(\mathbf{s}) + \frac{1}{2}Q_{\mathbf{p}}(\mathbf{s}) + O(\|\mathbf{s}\|_2^3). \quad (11)$$

Equation (11) links *intrinsic coordinates* to *extrinsic coordinates* for  $\mathcal{M}$ , where

- $L_{\mathbf{p}} : T_{\mathbf{p}}\mathcal{M} \rightarrow \mathbb{R}^D$  is a homogeneous linear function, the *differential* of the exponential map at  $\mathbf{p}$ ,  $D\exp_{\mathbf{p}}(0)$ ;
- $Q_{\mathbf{p}} : T_{\mathbf{p}}\mathcal{M} \rightarrow \mathbb{R}^D$  is a homogeneous quadratic function, called the *second fundamental form* of  $\mathcal{M}$  at  $\mathbf{p}$  (see [44]).

We refer to

$$L_{\mathbf{p}}(T_{\mathbf{p}}\mathcal{M}) = \{L_{\mathbf{p}}(\mathbf{s}) : \mathbf{s} \in T_{\mathbf{p}}\mathcal{M}\} \subseteq \mathbb{R}^D, \quad (12)$$

$$\mathbf{p} + L_{\mathbf{p}}(T_{\mathbf{p}}\mathcal{M}) = \{\mathbf{p} + L_{\mathbf{p}}(\mathbf{s}) : \mathbf{s} \in T_{\mathbf{p}}\mathcal{M}\} \subseteq \mathbb{R}^D \quad (13)$$

as the *linear (resp., affine) embedded tangent space* of  $\mathcal{M}$  at  $\mathbf{p}$ . It is known that  $L_{\mathbf{p}}$  gives an *isometric embedding* of  $T_{\mathbf{p}}\mathcal{M}$  into  $\mathbb{R}^D$ , i.e., for all  $\mathbf{s} \in T_{\mathbf{p}}\mathcal{M}$ ,

$$\|L_{\mathbf{p}}(\mathbf{s})\|_2 = \|\mathbf{s}\|_2. \quad (14)$$

---

<sup>1</sup> Explicitly: for each  $\mathbf{s} \in T_{\mathbf{p}}\mathcal{M}$ , if we write  $\gamma_{\mathbf{s}} : \mathbb{R} \rightarrow \mathcal{M} \hookrightarrow \mathbb{R}^D$  for the curve  $t \mapsto \iota \circ \exp_{\mathbf{p}}(t\mathbf{s})$ , then  $\gamma_{\mathbf{s}}(0) = \mathbf{p}$ ,  $\gamma'_{\mathbf{s}}(0) = L_{\mathbf{p}}(\mathbf{s})$ , and  $\text{Proj}_{\gamma_{\mathbf{s}}(t)}(\gamma''_{\mathbf{s}}(t)) = 0$  for all  $t \in \mathbb{R}$ , where  $\text{Proj}_{\gamma_{\mathbf{s}}(t)} : \mathbb{R}^D \rightarrow L_{\gamma_{\mathbf{s}}(t)}(T_{\gamma_{\mathbf{s}}(t)}\mathcal{M})$  denotes orthogonal projection (see (11) and (12)).

Another important fact is that the second fundamental form takes values in the *normal space* to  $\mathcal{M}$  at  $\mathbf{p}$ ,  $L_{\mathbf{p}}(T_{\mathbf{p}}\mathcal{M})^\perp \subseteq \mathbb{R}^D$ , i.e., for all  $\mathbf{s}, \mathbf{s}' \in T_{\mathbf{p}}\mathcal{M}$ ,

$$\langle L_{\mathbf{p}}(\mathbf{s}), Q_{\mathbf{p}}(\mathbf{s}') \rangle_{\mathbb{R}^D} = 0. \quad (15)$$

Finally, we let  $\mu$  denote the *density* on  $\mathcal{M}$  uniquely determined by the Riemannian structure on  $\mathcal{M}$  inherited from  $\mathbb{R}^D$  (see [35, Proposition 16.45]). The density determines a measure on  $\mathcal{M}$ , which we refer to as the *uniform measure*. Also,  $\mu$  enables integration of measurable functions  $f : \mathcal{M} \rightarrow \mathbb{R}$ ,

$$\int_{\mathcal{M}} f(\mathbf{x}) d\mu(\mathbf{x}). \quad (16)$$

In particular,

$$\text{vol}(\mathcal{M}) := \int_{\mathcal{M}} 1 d\mu(\mathbf{x}) \in \mathbb{R}_{>0} \quad (17)$$

is the (Riemannian,  $d$ -dimensional) *volume* of  $\mathcal{M}$ .

## 2.2 Notation and preliminaries from convex geometry

Here we give a reminder on general norms in finite-dimensional vector spaces, and their equivalence with certain convex bodies. A few facts about tangent cones are also recorded. We recommend [25] for details on convex geometry.

Let  $\|\cdot\| : \mathbb{R}^D \rightarrow \mathbb{R}$  denote an *arbitrary vector space norm* on  $\mathbb{R}^D$ , i.e.,

- $\|\mathbf{v}\| \geq 0$  for all  $\mathbf{v} \in \mathbb{R}^D$ ;
- $\|\lambda\mathbf{v}\| = |\lambda|\|\mathbf{v}\|$  for all  $\lambda \in \mathbb{R}$  and  $\mathbf{v} \in \mathbb{R}^D$ ;
- $\|\mathbf{u} + \mathbf{v}\| \leq \|\mathbf{u}\| + \|\mathbf{v}\|$  for all  $\mathbf{u}, \mathbf{v} \in \mathbb{R}^D$ .

It is easy to see that  $\|\cdot\|$  is a continuous function on  $\mathbb{R}^D$ , and that all norms on  $\mathbb{R}^D$  are *strongly equivalent*. The latter means: if  $\|\cdot\|$  is another norm on  $\mathbb{R}^D$ , there exist finite positive constants  $c, C$  (depending on  $\|\cdot\|, \|\cdot\|$ ) such that

$$c\|\mathbf{v}\| \leq \|\mathbf{v}\| \leq C\|\mathbf{v}\| \text{ for all } \mathbf{v} \in \mathbb{R}^D. \quad (18)$$

Here is a familiar example. Let  $p \geq 1$  and  $\mathbf{w} = (w_1, \dots, w_D)^\top \in (\mathbb{R}_{>0})^D$ . Then, the following defines a norm on  $\mathbb{R}^D$ , called the  *$\mathbf{w}$ -weighted  $\ell_p$ -norm*,

$$\|\mathbf{v}\|_{\mathbf{w},p} := \left( \sum_{i=1}^D w_i |v_i|^p \right)^{1/p} \text{ for } \mathbf{v} = (v_1, \dots, v_D)^\top \in \mathbb{R}^D. \quad (19)$$

We emphasize, however, that an arbitrary norm  $\|\cdot\|$  on  $\mathbb{R}^D$  is significantly more general than (19); indeed, it is essentially an object of convex geometry.

To this end, let us write  $\mathcal{B} \subseteq \mathbb{R}^D$  for the *unit ball* with respect to  $\|\cdot\|$ ,

$$\mathcal{B} := \{\mathbf{v} \in \mathbb{R}^D : \|\mathbf{v}\| \leq 1\}. \quad (20)$$

Then,  $\mathcal{B}$  is a *convex body* in  $\mathbb{R}^D$ . This means: a compact convex subset of  $\mathbb{R}^D$  with non-empty interior. Furthermore, the unit ball is *origin-symmetric*, i.e.,  $\mathbf{v} \in \mathcal{B}$  implies  $-\mathbf{v} \in \mathcal{B}$  for all  $\mathbf{v} \in \mathbb{R}^D$ . Conversely, it is well-known that any origin-symmetric convex body in  $\mathbb{R}^D$  occurs as the unit ball for some norm on  $\mathbb{R}^D$ . The conclusion is that norms and origin-symmetric convex bodies are in one-to-one correspondence [25, Chapter 2].

A few general topological remarks follow. Given any subset  $\mathcal{Y} \subseteq \mathbb{R}^D$ . The *topological boundary* of  $\mathcal{Y}$  is the closure of  $\mathcal{Y}$  minus the interior of  $\mathcal{Y}$ , written  $\partial\mathcal{Y} := \overline{\mathcal{Y}} \setminus \mathcal{Y}^\circ$ . In the case of the unit ball (20), the boundary is the *unit sphere*:

$$\partial\mathcal{B} = \{\mathbf{v} \in \mathbb{R}^D : \|\mathbf{v}\| = 1\}. \quad (21)$$

Now, given any point  $\mathbf{y} \in \mathcal{Y}$ . The *tangent cone to  $\mathcal{Y}$  at  $\mathbf{y}$*  is defined to be

$$TC_{\mathbf{y}}(\mathcal{Y}) := \left\{ \mathbf{d} \in \mathbb{R}^D : \exists (\mathbf{y}_k)_{k=1}^\infty \subseteq \mathcal{Y}, (\tau_k)_{k=1}^\infty \subseteq \mathbb{R}_{>0} \text{ s.t. } \tau_k \rightarrow 0, \frac{\mathbf{y}_k - \mathbf{y}}{\tau_k} \rightarrow \mathbf{d} \right\}. \quad (22)$$

It is obvious that  $TC_{\mathbf{y}}(\mathcal{Y})$  is indeed a *cone*. This means:  $0 \in TC_{\mathbf{y}}(\mathcal{Y})$  and  $\mathbf{d} \in TC_{\mathbf{y}}(\mathcal{Y})$ ,  $\lambda \in \mathbb{R}_{\geq 0}$  imply  $\lambda\mathbf{d} \in TC_{\mathbf{y}}(\mathcal{Y})$ . Further,  $TC_{\mathbf{y}}(\mathcal{Y})$  is a closed set. For convex  $\mathcal{Y}$ , the following explicit description is available [49, Lemma 3.13],

$$TC_{\mathbf{y}}(\mathcal{Y}) = \overline{\mathbb{R}_{>0}(\mathcal{Y} - \mathbf{y})} := \overline{\{\beta(\tilde{\mathbf{y}} - \mathbf{y}) \in \mathbb{R}^D : \beta \in \mathbb{R}_{>0}, \tilde{\mathbf{y}} \in \mathcal{Y}\}}. \quad (23)$$

In particular, if  $\mathcal{Y}$  is convex (respectively, convex with non-empty interior), then  $TC_{\mathbf{y}}(\mathcal{Y})$  is convex (respectively, convex with non-empty interior).

For purposes of the next subsection, we note that the topological boundary and tangent cone operations commute, at least in the case of our interest.

**Lemma 1** For  $\mathcal{B} \subseteq \mathbb{R}^D$  the unit ball of a norm  $\|\cdot\|$  and  $\mathbf{y} \in \partial\mathcal{B}$ ,

$$\partial(TC_{\mathbf{y}}(\mathcal{B})) = TC_{\mathbf{y}}(\partial\mathcal{B}). \quad (24)$$

We prove Lemma 1 in Appendix A, as we could not find this in the literature.

Preparing for the next subsection, we also record an easy remark/example.

*Remark 2* The closed convex cones in  $\mathbb{R}^2$  with non-empty interior are precisely  $\mathbb{R}^2$  and the *conical hull* of two linearly independent vectors  $\mathbf{d}_1, \mathbf{d}_2 \in \mathbb{R}^2$ ,

$$\text{coni}\{\mathbf{d}_1, \mathbf{d}_2\} := \{\beta_1\mathbf{d}_1 + \beta_2\mathbf{d}_2 : \beta_1, \beta_2 \in \mathbb{R}_{\geq 0}\} \subseteq \mathbb{R}^2. \quad (25)$$

In the latter case,  $\mathbf{d}_1, \mathbf{d}_2$  are unique up to positive scale, and one says that they generate the cone's *extremal rays*,  $\text{coni}\{\mathbf{d}_1\}$  and  $\text{coni}\{\mathbf{d}_2\}$ .

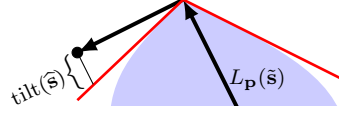


**Fig. 1** *Tilt construction.* This picture takes place in a 2D linear subspace of  $\mathbb{R}^D$ ,  $\mathcal{S} = \text{Span}(L_{\mathbf{p}}(\hat{\mathbf{s}}), Q_{\mathbf{p}}(\hat{\mathbf{s}}))$ , where  $L_{\mathbf{p}}(\hat{\mathbf{s}})$  and  $Q_{\mathbf{p}}(\hat{\mathbf{s}})$  are tangent and normal, respectively, to  $\mathcal{M}$  at  $\mathbf{p}$ . Blue shows the 2D slice of  $\|\cdot\|$ 's unit ball,  $\tilde{\mathcal{B}} = \mathcal{B} \cap \mathcal{S}$ . Red shows the tangents to  $\partial\tilde{\mathcal{B}}$  at  $L_{\mathbf{p}}(\hat{\mathbf{s}})$ , where  $\hat{\mathbf{s}} := \mathbf{s}/\|\mathbf{s}\|$  for convenience. Here, the tilt function  $\text{tilt}_{\mathcal{M}, \mathcal{B}, \mathbf{p}}(\hat{\mathbf{s}})$  equals the signed  $\ell_2$ -length of the braced line segment. In this case, *tilt* is negative (inward pointing).

### 2.3 Tilt construction

Here we record a novel construction that turns out to be important in expressing the limiting differential operator of Theorem 1. Let  $\mathcal{M} \subseteq \mathbb{R}^D$  be a compact smooth embedded Riemannian manifold,  $\mathbf{p} \in \mathcal{M}$  a point, and  $\|\cdot\|$  an (arbitrary) norm on  $\mathbb{R}^D$  with unit ball  $\mathcal{B}$ . We will construct a scalar-valued function  $\text{tilt}_{\mathcal{M}, \mathcal{B}, \mathbf{p}}$ , whose inputs are normalized tangent vectors in  $T_{\mathbf{p}}\mathcal{M}$ , which captures a “second-order interaction” between the manifold  $\mathcal{M}$  and the unit ball  $\mathcal{B}$  (Proposition/Definition 1). The meaning of this is depicted in Figure 1.

**Proposition/Definition 1** *Let  $\hat{\mathbf{s}} \in T_{\mathbf{p}}\mathcal{M}$  with  $\|\hat{\mathbf{s}}\|_2 = 1$ . Set  $\mathbf{a} = L_{\mathbf{p}}(\hat{\mathbf{s}})$  and  $\mathbf{b} = \frac{1}{2}Q_{\mathbf{p}}(\hat{\mathbf{s}})$ . Then there exists a unique  $\eta \in \mathbb{R}$  such that*

$$\frac{\mathbf{b}}{\|\mathbf{a}\|^2} + \eta\mathbf{a} \in TC_{\mathbf{a}/\|\mathbf{a}\|}(\partial\mathcal{B}). \quad (26)$$

We define  $\text{tilt}_{\mathcal{M}, \mathcal{B}, \mathbf{p}}(\hat{\mathbf{s}}) := \eta$ .

*Proof* Let  $\mathcal{S} := \text{Span}\{\mathbf{a}, \mathbf{b}\} \subseteq \mathbb{R}^D$ . For each  $\eta \in \mathbb{R}$ , the LHS of (26) lies in  $\mathcal{S}$ , so, the membership (26) is equivalent to

$$\frac{\mathbf{b}}{\|\mathbf{a}\|^2} + \eta\mathbf{a} \in \mathcal{S} \cap TC_{\mathbf{a}/\|\mathbf{a}\|}(\partial\mathcal{B}). \quad (27)$$

We simplify the RHS of (27). Commuting tangent cones and boundaries by Lemma 1,

$$\mathcal{S} \cap TC_{\mathbf{a}/\|\mathbf{a}\|}(\partial\mathcal{B}) = \mathcal{S} \cap \partial(TC_{\mathbf{a}/\|\mathbf{a}\|}(\mathcal{B})). \quad (28)$$

Using that  $TC_{\mathbf{a}/\|\mathbf{a}\|}(\mathcal{B})$  is a closed set,

$$\mathcal{S} \cap \partial(TC_{\mathbf{a}/\|\mathbf{a}\|}(\mathcal{B})) = \partial_{\text{rel}}(\mathcal{S} \cap TC_{\mathbf{a}/\|\mathbf{a}\|}(\mathcal{B})), \quad (29)$$

where in the RHS,  $\partial_{\text{rel}}$  is to be understood using relative interior (this means: we regard  $\mathcal{S} \cap TC_{\mathbf{a}/\|\mathbf{a}\|}(\mathcal{B})$  as a subset of  $\mathcal{S}$  when taking interior). From properties of tangent cones of intersections [8, Proposition 3.36],

$$\partial_{\text{rel}}(\mathcal{S} \cap TC_{\mathbf{a}/\|\mathbf{a}\|}(\mathcal{B})) = \partial_{\text{rel}}(TC_{\mathbf{a}/\|\mathbf{a}\|}(\tilde{\mathcal{B}})), \quad (30)$$



where  $\tilde{\mathcal{B}} := \mathcal{S} \cap \mathcal{B}$ . Let us note  $\tilde{\mathcal{B}}$  is the unit ball of  $\|\cdot\|$  restricted to  $\mathcal{S}$ , and the RHS of (30) is nothing but the boundary of a convex tangent cone in  $\mathcal{S}$ .

At this point, recall  $\mathbf{a} \neq 0$  by the isometry property (14), and  $\langle \mathbf{a}, \mathbf{b} \rangle = 0$  by the normality property (15). If  $\mathbf{b} = 0$  then  $\mathcal{S} = \text{Span}\{\mathbf{a}\} \cong \mathbb{R}$ ,  $\tilde{\mathcal{B}}$  is a line segment,  $TC_{\mathbf{a}/\|\mathbf{a}\|}(\tilde{\mathcal{B}})$  is a ray, and  $\partial_{\text{rel}}(TC_{\mathbf{a}/\|\mathbf{a}\|}(\tilde{\mathcal{B}}))$  is the origin, and so (26) uniquely determines  $\eta = 0$ .

Thus, assume  $\mathbf{b} \neq 0$ , so  $\mathcal{S} \cong \mathbb{R}^2$ . We claim  $TC_{\mathbf{a}/\|\mathbf{a}\|}(\tilde{\mathcal{B}}) \neq \mathbb{R}^2$ . By convexity of  $\tilde{\mathcal{B}}$  and the supporting hyperplane theorem,

$$\exists \mathbf{v} \in \mathcal{S} \setminus \{0\}, \exists \gamma \in \mathbb{R} \text{ such that } \langle \mathbf{v}, \mathbf{a}/\|\mathbf{a}\| \rangle = \gamma \text{ and } \forall \mathbf{u} \in \tilde{\mathcal{B}}, \langle \mathbf{v}, \mathbf{u} \rangle \geq \gamma. \quad (31)$$

It follows  $TC_{\mathbf{a}/\|\mathbf{a}\|}(\tilde{\mathcal{B}}) \subseteq \{\mathbf{d} \in \mathcal{S} : \langle \mathbf{v}, \mathbf{d} \rangle \geq 0\}$ , so  $TC_{\mathbf{a}/\|\mathbf{a}\|}(\tilde{\mathcal{B}}) \neq \mathbb{R}^2$  indeed. We can now apply Remark 2 to get

$$TC_{\mathbf{a}/\|\mathbf{a}\|}(\tilde{\mathcal{B}}) = \text{coni}\{\mathbf{d}_1, \mathbf{d}_2\}, \quad (32)$$

for linearly independent  $\mathbf{d}_1, \mathbf{d}_2 \in \mathcal{S}$ . Then, clearly

$$\partial_{\text{rel}}(TC_{\mathbf{a}/\|\mathbf{a}\|}(\tilde{\mathcal{B}})) = \text{coni}\{\mathbf{d}_1\} \cup \text{coni}\{\mathbf{d}_2\}. \quad (33)$$

We have argued that  $\mathcal{S} \cap TC_{\mathbf{a}/\|\mathbf{a}\|}(\partial\mathcal{B})$  (26) is the union of two rays (33) (assuming  $\mathbf{b} \neq 0$ ).

On the other hand, by the description of tangent cones to convex sets (23),

$$-\mathbf{a} \in \left(TC_{\mathbf{a}/\|\mathbf{a}\|}(\tilde{\mathcal{B}})\right)^\circ, \quad (34)$$

where again relative interior is understood.

Combining (32) and (34) with  $\langle \mathbf{a}, \mathbf{b} \rangle = 0$ , it follows there exists exactly one index  $i \in \{1, 2\}$  such that  $\langle \mathbf{d}_i, \mathbf{b} \rangle > 0$ , while  $\langle \mathbf{d}_j, \mathbf{b} \rangle < 0$  for  $j = \{1, 2\} \setminus \{i\}$ . Relabeling if necessary,  $i = 1$ .

Now, consider

$$\frac{\mathbf{b}}{\|\mathbf{a}\|^2} + \eta \mathbf{a} \in \text{coni}\{\mathbf{d}_1\} \cup \text{coni}\{\mathbf{d}_2\}. \quad (35)$$

For all  $\eta \in \mathbb{R}$  and  $\beta \in \mathbb{R}_{\geq 0}$ , we have

$$\frac{\mathbf{b}}{\|\mathbf{a}\|^2} + \eta \mathbf{a} \neq \beta \mathbf{d}_2, \quad (36)$$

by comparing the inner product of each side with  $\mathbf{b}$ . However, there do exist  $\eta \in \mathbb{R}$  and  $\beta \in \mathbb{R}_{\geq 0}$  satisfying

$$\frac{\mathbf{b}}{\|\mathbf{a}\|^2} + \eta \mathbf{a} = \beta \mathbf{d}_1. \quad (37)$$

Taking inner products with  $\mathbf{a}$  and  $\mathbf{b}$ , we compute the following *unique* solution:

$$\beta = \|\mathbf{b}\|_2^2 / (\|\mathbf{a}\|^2 \langle \mathbf{d}_1, \mathbf{b} \rangle) \in \mathbb{R}_{>0}, \quad (38)$$

$$\eta = \|\mathbf{b}\|_2^2 \langle \mathbf{a}, \mathbf{d}_1 \rangle / (\|\mathbf{a}\|^2 \langle \mathbf{d}_1, \mathbf{b} \rangle) \in \mathbb{R}. \quad (39)$$

This completes the proof that  $\eta$  exists and is unique. In conclusion,  $\text{tilt}_{\mathcal{M}, \mathcal{B}, \mathbf{p}}(\hat{\mathbf{s}})$  is given by the formula (39).  $\square$

*Remark 3* We try to unpack the tilt construction. First, note  $\text{tilt}_{\mathcal{M}, \mathcal{B}, \mathbf{p}}(\hat{\mathbf{s}})$  depends only on a particular linear section of the unit ball of  $\|\cdot\|$  spanned by the tangent vector  $L_{\mathbf{p}}(\hat{\mathbf{s}})$  and the normal vector  $Q_{\mathbf{p}}(\hat{\mathbf{s}})$ ,

$$\tilde{\mathcal{B}} = \text{Span}\{L_{\mathbf{p}}(\hat{\mathbf{s}}), Q_{\mathbf{p}}(\hat{\mathbf{s}})\} \cap \mathcal{B}. \quad (40)$$

If the second fundamental form of  $\mathcal{M}$  vanishes at  $\hat{\mathbf{s}}$ , i.e.,  $Q_{\mathbf{p}}(\hat{\mathbf{s}}) = 0$ , then  $\text{tilt}_{\mathcal{M}, \mathcal{B}, \mathbf{p}}(\hat{\mathbf{s}}) = 0$ . Otherwise,  $\tilde{\mathcal{B}}$  is a two-dimensional slice of  $\mathcal{B}$ , and so an origin-symmetric convex body in  $\mathbb{R}^2$ . According to formula (39),  $\text{tilt}_{\mathcal{M}, \mathcal{B}, \mathbf{p}}(\hat{\mathbf{s}})$  is determined by the orientation of the extremal rays of

$$TC_{L_{\mathbf{p}}(\hat{\mathbf{s}})/\|L_{\mathbf{p}}(\hat{\mathbf{s}})\|}(\tilde{\mathcal{B}}) \quad (41)$$

with respect to  $L_{\mathbf{p}}(\hat{\mathbf{s}})$  and  $Q_{\mathbf{p}}(\hat{\mathbf{s}})$ , as well as the magnitudes  $\|L_{\mathbf{p}}(\hat{\mathbf{s}})\|, \|Q_{\mathbf{p}}(\hat{\mathbf{s}})\|_2$ .

It will be convenient to allow an abuse of notation, by permitting an isomorphic domain of normalized tangent vectors for the tilt function.

**Definition 1** Let  $\hat{\mathbf{t}} \in \mathbb{R}^D$  with  $\hat{\mathbf{t}} \in \partial\mathcal{B} \cap L_{\mathbf{p}}(T_{\mathbf{p}}\mathcal{M})$ . There is a unique  $\hat{\mathbf{s}} \in T_{\mathbf{p}}\mathcal{M}$  with  $\|\hat{\mathbf{s}}\|_2 = 1$  such that

$$\hat{\mathbf{t}} = \frac{L_{\mathbf{p}}(\hat{\mathbf{s}})}{\|L_{\mathbf{p}}(\hat{\mathbf{s}})\|}. \quad (42)$$

By abuse of notation, define  $\text{tilt}_{\mathcal{M}, \mathcal{B}, \mathbf{p}}(\hat{\mathbf{t}}) := \text{tilt}_{\mathcal{M}, \mathcal{B}, \mathbf{p}}(\hat{\mathbf{s}}) \in \mathbb{R}$ .

## 2.4 Theorem statement

Here we state the main result of this paper. It is a determination of the limiting second-order differential operator arises from Laplacian-based manifold learning with respect to an arbitrary norm (Theorem 1 and Definition 2).

For  $\sigma > 0$ , let  $K_{\sigma} : \mathbb{R}_{\geq 0} \rightarrow \mathbb{R}_{> 0}$  denote the  $\sigma$ -bandwidth Gaussian kernel,

$$K_{\sigma}(t) := \exp\left(\frac{-t^2}{\sigma^2}\right). \quad (43)$$

Also, write  $\Gamma : \mathbb{R}_{> 0} \rightarrow \mathbb{R}_{> 0}$  for the gamma function,  $\Gamma(z) := \int_0^{\infty} x^{z-1} e^{-x} dx$ .

**Theorem 1** Let  $\|\cdot\| : \mathbb{R}^D \rightarrow \mathbb{R}_{\geq 0}$  be an arbitrary norm, with unit ball  $\mathcal{B}$  and unit sphere  $\partial\mathcal{B}$ . Let  $\mathcal{M} \subseteq \mathbb{R}^D$  be a compact smooth Riemannian manifold of dimension  $d$  (embedded with respect to the Euclidean structure in  $\mathbb{R}^D$ ). Fix a point  $\mathbf{p} \in \mathcal{M}$  and a  $C^3$  function  $f : \mathcal{M} \rightarrow \mathbb{R}$ . Let  $\mathbf{x}_1, \dots, \mathbf{x}_n$  be i.i.d. draws from the uniform measure on  $\mathcal{M}$  (given by the Riemannian density on  $\mathcal{M}$ ). Put

$\sigma_n := n^{-1/(2d+4+\alpha)}$  where  $\alpha > 0$  is any constant, and  $C_n := 1/(\Gamma(\frac{d+4}{2})\sigma_n^{d+2})$ . Then the following convergence holds in probability:

$$\begin{aligned} & \lim_{n \rightarrow \infty} \text{vol}(\mathcal{M})(C_n/n) \sum_{i=1}^n K_{\sigma_n}(\|\mathbf{x}^{(i)} - \mathbf{p}\|)(f(\mathbf{x}^{(i)}) - f(\mathbf{p})) \\ &= \left\langle \nabla^2 \tilde{f}(0), \frac{1}{2} \int_{\{\mathbf{s} \in T_{\mathbf{p}}\mathcal{M} : \|L_{\mathbf{p}}(\mathbf{s})\| \leq 1\}} \mathbf{s}\mathbf{s}^\top d\mathbf{s} \right\rangle + \\ & \left\langle \nabla \tilde{f}(0), \int_{\{\hat{\mathbf{s}} \in T_{\mathbf{p}}\mathcal{M} : \|\hat{\mathbf{s}}\|_2 = 1\}} \hat{\mathbf{s}} \|L_{\mathbf{p}}(\hat{\mathbf{s}})\|^{-d} \text{tilt}_{\mathcal{M}, \mathcal{B}, \mathbf{p}}(\hat{\mathbf{s}}) d\hat{\mathbf{s}} \right\rangle, \end{aligned} \quad (44)$$

where  $\tilde{f} := f \circ \exp_{\mathbf{p}} : T_{\mathbf{p}}\mathcal{M} \rightarrow \mathbb{R}$  and  $L_{\mathbf{p}} = D\exp_{\mathbf{p}}(0) : T_{\mathbf{p}}\mathcal{M} \rightarrow \mathbb{R}^D$ .

For safety, we clarify (44): the angled brackets denote Frobenius inner product of  $d \times d$  matrices and the Euclidean inner product on  $T_{\mathbf{p}}\mathcal{M} \cong \mathbb{R}^d$ , respectively. Also,  $\nabla$  and  $\nabla^2$  are the usual gradient and Hessian operators, and  $d\mathbf{s}$  and  $d\hat{\mathbf{s}}$  denote the Lebesgue measures on  $T_{\mathbf{p}}\mathcal{M}$  and  $\{\hat{\mathbf{s}} \in T_{\mathbf{p}}\mathcal{M} : \|\hat{\mathbf{s}}\|_2 = 1\}$ .

**Definition 2** Define  $\mathcal{L}_{\mathcal{M}, \|\cdot\|}$  to be the second-order linear differential operator<sup>2</sup> on  $\mathcal{M}$  such that for all  $f \in C^3(\mathcal{M})$ , the RHS of (44) equals  $\mathcal{L}_{\mathcal{M}, \|\cdot\|}(f)(\mathbf{p})$ . We call  $\mathcal{L}_{\mathcal{M}, \|\cdot\|}$  the *Laplacian-like operator of  $\mathcal{M} \subseteq \mathbb{R}^D$  with respect to  $\|\cdot\|$* .

As for the LHS of Equation (44), it consists of discrete graph Laplacians computed using the norm  $\|\cdot\|$  and applied to randomly sampled versions of  $f$ ,

$$\mathcal{L}_{\mathcal{M}, \|\cdot\|}^{(n)}(f)(\mathbf{p}) := \text{vol}(\mathcal{M})(C_n/n) \sum_{i=1}^n K_{\sigma_n}(\|\mathbf{x}^{(i)} - \mathbf{p}\|)(f(\mathbf{x}^{(i)}) - f(\mathbf{p})) \quad (45)$$

(recall Subsection 1.2). We can restate Theorem 1 as weak convergence of operators; this is nothing but terminology, but we think it aids in understanding.

**Theorem 1 (restated in terms of operators)** *Assume the same setup as in Theorem 1 above. Then there is the following weak convergence of operators in probability:*

$$\mathcal{L}_{\mathcal{M}, \|\cdot\|}^{(n)} \longrightarrow \mathcal{L}_{\mathcal{M}, \|\cdot\|} \quad \text{as } n \rightarrow \infty. \quad (46)$$

*This convergence is in the sense: for each fixed  $C^3$  function  $f : \mathcal{M} \rightarrow \mathbb{R}$  and point  $\mathbf{p} \in \mathcal{M}$ , we have  $\mathcal{L}_{\mathcal{M}, \|\cdot\|}^{(n)}(f)(\mathbf{p}) \rightarrow \mathcal{L}_{\mathcal{M}, \|\cdot\|}(f)(\mathbf{p})$  as  $n \rightarrow \infty$  in probability.*

We can also re-express the integrals appearing in (44) directly in  $\mathbb{R}^D$ . As written above, Theorem 1 expresses the limiting differential operator in geodesic normal coordinates. However, substituting  $\mathbf{t} = L_{\mathbf{p}}(\mathbf{s})$ ,  $\hat{\mathbf{t}} = L_{\mathbf{p}}(\hat{\mathbf{s}})/\|L_{\mathbf{p}}(\hat{\mathbf{s}})\|$  and recalling that  $L_{\mathbf{p}}$  is an isometry, we get the following.

<sup>2</sup> It is easy to see directly from the RHS of (44) that  $\mathcal{L}_{\mathcal{M}, \|\cdot\|}$  is an elliptic differential operator on  $\mathcal{M}$ , for all  $\mathcal{M}$  and  $\|\cdot\|$ .

**Theorem 1 (with integrals re-expressed in  $\mathbb{R}^D$ )** *Assume the same setup as in Theorem 1 above. Then there is the following convergence in probability:*

$$\begin{aligned} & \lim_{n \rightarrow \infty} \text{vol}(\mathcal{M})(C_n/n) \sum_{i=1}^n K_{\sigma_n}(\|\mathbf{x}^{(i)} - \mathbf{p}\|)(f(\mathbf{x}^{(i)}) - f(\mathbf{p})) \\ &= \left\langle L_{\mathbf{p}} \nabla^2 \tilde{f}(0) L_{\mathbf{p}}^\top, \frac{1}{2} \int_{\mathbf{t} \in L_{\mathbf{p}}(T_{\mathbf{p}}\mathcal{M}) \cap \mathcal{B}} \mathbf{t} \mathbf{t}^\top d\mathbf{t} \right\rangle + \\ & \left\langle L_{\mathbf{p}} \nabla \tilde{f}(0), \int_{\hat{\mathbf{t}} \in L_{\mathbf{p}}(T_{\mathbf{p}}\mathcal{M}) \cap \partial\mathcal{B}} \hat{\mathbf{t}} \text{tilt}_{\mathcal{M}, \mathcal{B}, \mathbf{p}}(\hat{\mathbf{t}}) d\hat{\mathbf{t}} \right\rangle, \end{aligned} \quad (47)$$

where  $d\mathbf{t}$  and  $d\hat{\mathbf{t}}$  are the pushforwards of  $d\mathbf{s}$  and  $d\hat{\mathbf{s}}$  under  $\mathbf{s} \mapsto L_{\mathbf{p}}(\mathbf{s})$  and  $\hat{\mathbf{s}} \mapsto L_{\mathbf{p}}(\hat{\mathbf{s}})/\|L_{\mathbf{p}}(\hat{\mathbf{s}})\|$ , respectively.

Now the angled brackets denote Frobenius inner product of  $D \times D$  matrices and the Euclidean inner product on  $\mathbb{R}^D$ , respectively.

*Remark 4* Let us interpret (47)'s expression of the limiting differential operator. The integral in the second-order term represents the second moment of the unit ball of the norm  $\|\cdot\|$  intersected with the linear embedded tangent space of the manifold  $\mathcal{M}$  at the point  $\mathbf{p}$ ; that is, the second moment of  $L_{\mathbf{p}}(T_{\mathbf{p}}\mathcal{M}) \cap \mathcal{B}$ , a certain  $d$ -dimensional convex body in  $\mathbb{R}^D$ . Meanwhile, the integral in the first-order term runs over the  $(d-1)$ -dimensional boundary of this body,  $L_{\mathbf{p}}(T_{\mathbf{p}}\mathcal{M}) \cap \partial\mathcal{B}$ . This integral is the weighted first moment of the boundary, with weighting according to the tilt function  $\text{tilt}_{\mathcal{M}, \mathcal{B}, \mathbf{p}}$ .

*Remark 5* It is important to note our result shows that the limit of graph Laplacians with respect to general norms typically behaves quite differently to the Laplace-Beltrami operator. The limit is typically extrinsic: both terms in (47) vary with the orientation of the tangent space  $L_{\mathbf{p}}(T_{\mathbf{p}}\mathcal{M}) \subseteq \mathbb{R}^D$  in relation to the unit ball  $\mathcal{B} \subseteq \mathbb{R}^D$ . Further, there is typically a first-order derivative term in  $\mathcal{L}_{\mathcal{M}, \|\cdot\|}$ . In both respects, the  $\ell_2$  norm is special: it gives rise to the Laplace-Beltrami operator on  $\mathcal{M}$ , which is intrinsic and carries no first-derivative term.

Finally, we note that the uniform sampling assumption in the theorem is not as severe as it might seem (details left to the reader).

**Corollary 1** *Assume the same setup as Theorem 1 above, except  $\mathbf{x}_1, \dots, \mathbf{x}_n$  are i.i.d. draws from a probability distribution on  $\mathcal{M}$  possessing a  $C^3$  probability density function,  $dP(\mathbf{x}) = P(\mathbf{x})d\mu(\mathbf{x})$ . Define  $h : \mathcal{M} \rightarrow \mathbb{R}$  by  $h(\mathbf{x}) := (f(\mathbf{x}) - f(\mathbf{p}))P(\mathbf{x})$ . Then, the limit in the RHS of (44) becomes*

$$\mathcal{L}_{\mathcal{M}, \|\cdot\|}(h)(\mathbf{p}), \quad (48)$$

by the same straightforward reduction as in [6, Section 5].

## 2.5 Example: any manifold, Euclidean norm

Let us first check that our theory reduces correctly to the standard Euclidean case. Let  $\mathcal{M} \subseteq \mathbb{R}^D$  be any  $d$ -dimensional compact smooth embedded Riemannian manifold,  $\mathbf{p} \in \mathcal{M}$ , and consider the Euclidean norm  $\|\cdot\| = \|\cdot\|_2$  with Euclidean unit ball  $\mathcal{B} \subseteq \mathbb{R}^D$ .

We first argue  $\text{tilt}_{\mathcal{M}, \mathcal{B}, \mathbf{p}} \equiv 0$ . Let  $\hat{\mathbf{s}} \in T_{\mathbf{p}}\mathcal{M}$  with  $\|\hat{\mathbf{s}}\|_2 = 1$ . Set  $\mathbf{a} = L_{\mathbf{p}}(\hat{\mathbf{s}})$ ,  $\mathbf{b} = \frac{1}{2}Q_{\mathbf{p}}(\hat{\mathbf{s}})$  and  $\mathcal{S} = \text{Span}\{\mathbf{a}, \mathbf{b}\}$ . If  $\mathbf{b} = 0$ , then  $\text{tilt}_{\mathcal{M}, \mathcal{B}, \mathbf{p}}(\hat{\mathbf{s}}) = 0$ . Else, put  $\tilde{\mathcal{B}} := \mathcal{B} \cap \mathcal{S}$ . By construction,  $\text{tilt}_{\mathcal{M}, \mathcal{B}, \mathbf{p}}(\hat{\mathbf{s}}) = \eta$  for  $\eta \in \mathbb{R}$  uniquely determined by

$$\mathbf{b} + \eta \mathbf{a} \in TC_{\mathbf{a}}(\partial \tilde{\mathcal{B}}), \quad (49)$$

using  $\|\mathbf{a}\|_2 = 1$  since  $L_{\mathbf{p}}$  is an isometry (14). However,  $\tilde{\mathcal{B}}$  is a Euclidean unit disk in  $\mathcal{S} \cong \mathbb{R}^2$ , and  $\partial \tilde{\mathcal{B}}$  is a Euclidean unit circle in  $\mathbb{R}^2$ . So,  $TC_{\mathbf{a}}(\partial \tilde{\mathcal{B}})$  is the orthogonal complement of  $\mathbb{R}\mathbf{a}$  inside  $\mathcal{S}$ . This gives  $TC_{\mathbf{a}}(\partial \tilde{\mathcal{B}}) = \mathbb{R}\mathbf{b}$  since  $Q_{\mathbf{p}}$  takes values in the normal space (15). Clearly then,  $\eta = 0$  and  $\text{tilt}_{\mathcal{M}, \mathcal{B}, \mathbf{p}} \equiv 0$ . We have verified that the first-order term vanishes in  $\mathcal{L}_{\mathcal{M}, \|\cdot\|_2}$ .

As for the second-order term, we compute the following second moment:

$$\begin{aligned} \int_{\{\mathbf{s} \in T_{\mathbf{p}}\mathcal{M} : \|L_{\mathbf{p}}(\mathbf{s})\|_2 \leq 1\}} \mathbf{s} \mathbf{s}^\top d\mathbf{s} &= \int_{\{\mathbf{s} \in T_{\mathbf{p}}\mathcal{M} : \|\mathbf{s}\|_2 \leq 1\}} \mathbf{s} \mathbf{s}^\top d\mathbf{s} && [\text{by (14)}] \\ &= \left( \int_{\{\mathbf{s} \in T_{\mathbf{p}}\mathcal{M} : \|\mathbf{s}\|_2 \leq 1\}} s_1^2 d\mathbf{s} \right) I_d && [\text{by oddness}] \\ &= (2^d/3) I_d. && (50) \end{aligned}$$

Here, the second equality used that  $\{\mathbf{s} \in T_{\mathbf{p}}\mathcal{M} : \|\mathbf{s}\|_2 \leq 1\}$  is closed under sign flips of individual coordinates of  $\mathbf{s}$ , whence off-diagonal terms  $s_i s_j$  with  $i \neq j$  integrate to 0.

Plugging into the RHS of (44),

$$\mathcal{L}_{\mathcal{M}, \|\cdot\|_2}(f)(\mathbf{p}) = \left\langle \nabla^2 \tilde{f}(0), (2^{d-1}/3) I_d \right\rangle \propto \text{trace} \left( \nabla^2 \tilde{f}(0) \right) \quad (51)$$

However, it is well-known

$$\text{trace} \left( \nabla^2 \tilde{f}(0) \right) = \Delta_{\mathcal{M}} f(\mathbf{p}), \quad (52)$$

where  $\Delta_{\mathcal{M}}$  is the Laplace-Beltrami operator on  $\mathcal{M}$ .

We have checked that Theorem 1 recovers  $\mathcal{L}_{\mathcal{M}, \|\cdot\|_2} \propto \Delta_{\mathcal{M}}$ .

## 2.6 Example: circle in the plane, weighted $\ell_1$ -norm

Next, we look at a non-Euclidean example in full detail. This illustrates some salient features of Laplacian-like operators with respect to general norms (see Remarks 5 and 6).

Consider the Euclidean unit circle in  $\mathbb{R}^2$ , and take  $\|\cdot\|$  to be a weighted  $\ell_1$ -norm. That is, let  $\mathcal{M} = S^1 = \{\mathbf{x} = (x_1, x_2)^\top \in \mathbb{R}^2 : x_1^2 + x_2^2 = 1\}$  and  $\|\cdot\| = \|\cdot\|_{\mathbf{w},1}$  where  $\mathbf{w} = (w_1, w_2)^\top \in (\mathbb{R}_{>0})^2$  so  $\|\mathbf{x}\|_{\mathbf{w},1} = w_1|x_1| + w_2|x_2|$  (recall (19)). The unit ball of  $\|\cdot\|_{\mathbf{w},1}$  is

$$\mathcal{B} = \{\mathbf{x} = (x_1, x_2)^\top \in \mathbb{R}^2 : w_1|x_1| + w_2|x_2| \leq 1\}, \quad (53)$$

the usual solid diamond, while the unit sphere of  $\|\cdot\|_{\mathbf{w},1}$  is

$$\partial\mathcal{B} = \{\mathbf{x} = (x_1, x_2)^\top \in \mathbb{R}^2 : w_1|x_1| + w_2|x_2| = 1\}, \quad (54)$$

a rhombus with vertices  $(\pm(1/w_1), 0), (0, \pm(1/w_2))$ .

Let  $\mathbf{p} = (\cos(\theta), \sin(\theta))^\top \in S^1$ . Parameterize  $T_{\mathbf{p}}S^1$  (with respect to a fixed unit basis vector) using  $\psi \in \mathbb{R}$ . The exponential map is

$$\exp_{\mathbf{p}} : T_{\mathbf{p}}S^1 \rightarrow S^1, \quad \psi \mapsto (\cos(\theta + \psi), \sin(\theta + \psi))^\top. \quad (55)$$

The differential of this is

$$L_{\mathbf{p}}(\psi) = \psi (-\sin(\theta), \cos(\theta))^\top. \quad (56)$$

The second fundamental form is

$$Q_{\mathbf{p}}(\psi) = -\psi^2 (\cos(\theta), \sin(\theta))^\top. \quad (57)$$

We take on the terms in the limiting operator in (44) in turn. For the second-order term, we need the second moment of a line segment:

$$\begin{aligned} \frac{1}{2} \int_{\{\psi : \|L_{\mathbf{p}}(\psi)\|_{\mathbf{w},1} \leq 1\}} \psi^2 d\psi &= \frac{1}{2} \int_{|\psi| \leq \|(-\sin(\theta), \cos(\theta))^\top\|_{\mathbf{w},1}^{-1}} \psi^2 d\psi \\ &= \frac{1}{3 (w_1|\sin(\theta)| + w_2|\cos(\theta)|)^3}. \end{aligned} \quad (58)$$

As for the first-order coefficient, this becomes a sum of over the two endpoints of the line segment. We shall show the first-order coefficient equals

$$\text{sign}(\cos(\theta)\sin(\theta)) \frac{-w_1|\cos(\theta)| + w_2|\sin(\theta)|}{(w_1|\sin(\theta)| + w_2|\cos(\theta)|)^4}, \quad (59)$$

where  $\text{sign} : \mathbb{R} \rightarrow \{-1, 0, 1\}$  is given by  $\text{sign}(t) := 1$  if  $t > 0$ ;  $\text{sign}(t) := -1$  if  $t < 0$ ; and  $\text{sign}(0) := 0$ . By the symmetry of the rhombus  $\partial\mathcal{B}$  with respect to individual coordinate sign flips in  $\mathbb{R}^2$ , one easily sees (59) is correct for  $\theta$  an integer multiple of  $\frac{\pi}{2}$  (the first-order coefficient is zero). Otherwise, we may reduce to  $\theta \in (0, \frac{\pi}{2})$ . Then, one can check it suffices to verify

$$\text{tilt}_{\mathcal{M}, \mathcal{B}, \mathbf{p}}(1) = \frac{1}{2} \frac{-w_1\cos(\theta) + w_2\sin(\theta)}{(w_1\sin(\theta) + w_2\cos(\theta))^3}. \quad (60)$$

To this end, let  $\alpha \in (0, \frac{\pi}{2})$  be half the angle  $\partial\mathcal{B}$  makes at  $(\frac{1}{w_1}, 0)^\top$ , so  $\tan(\alpha) = w_1/w_2$ . Let  $\mathbf{a} = L_{\mathbf{p}}(1)$  and  $\mathbf{b} = \frac{1}{2}Q_{\mathbf{p}}(1)$ . Let  $\omega$  be the signed angle at  $\mathbf{a}/\|\mathbf{a}\|_{\mathbf{w},1} \in \partial\mathcal{B}$  from  $\mathbf{a}/\|\mathbf{a}\|_{\mathbf{w},1} + \mathbb{R}_{\geq 0}(\frac{-1}{w_1}, \frac{-1}{w_2})^\top$  to  $\mathbf{a}/\|\mathbf{a}\|_{\mathbf{w},1} + \mathbb{R}_{\geq 0}\mathbf{b}$ ,

where counterclockwise counts as positive. By elementary angle chasing (details omitted),

$$\omega = \theta - \alpha. \quad (61)$$

Thus (see Figure 1),

$$\begin{aligned} \text{tilt}_{\mathcal{M}, \mathcal{B}, \mathbf{p}}(1) &= \left\| \frac{\mathbf{b}}{\|\mathbf{a}\|_{\mathbf{w},1}^2} \right\|_2 \tan(\omega) = \frac{1}{2\|\mathbf{a}\|_{\mathbf{w},1}^2} \tan(\theta - \alpha) \\ &= \frac{1}{2(w_1 \sin(\theta) + w_2 \cos(\theta))^2} \frac{\tan(\theta) - (w_1/w_2)}{1 + \tan(\theta)(w_1/w_2)}, \end{aligned} \quad (62)$$

which indeed simplifies to (60).

All together, for  $\theta \in [0, 2\pi]$ , we have checked Theorem 1 says  $\mathcal{L}_{S^1, \|\cdot\|_{\mathbf{w},1}}$  is

$$\text{sign}(\cos \theta \sin \theta) \frac{-w_1 |\cos \theta| + w_2 |\sin \theta|}{(w_1 |\sin \theta| + w_2 |\cos \theta|)^4} \frac{d}{d\theta} + \frac{1}{3(w_1 |\sin \theta| + w_2 |\cos \theta|)^3} \frac{d^2}{d\theta^2}. \quad (63)$$

It is reasonable to wonder if this formula actually checks out. Figure 2 displays numerical results in the affirmative. We fixed a particular  $f : S^1 \rightarrow \mathbb{R}$  (a trigonometric polynomial). Then we compared empirical graph Laplacians applied to  $f$  against the continuous operator (63) applied to  $f$ . As the sample size  $n$  grows, the empirical and theoretical plots matched up increasingly well.

*Remark 6* Notice that the coefficient function on the first-order differential operator  $\frac{d}{d\theta}$  is discontinuous at  $\theta = 0, \frac{\pi}{2}, \pi, \frac{3\pi}{2}$ . In fact, this shows the general behavior for Laplacian-like operators with respect to norms possessing points of non-differentiability in  $\mathbb{R}^D \setminus \{0\}$ .

In Appendix C, we present numerical results on the eigenfunctions of (63).

### 3 Proof of Theorem 1

To improve readability, we have organized the proof of Theorem 1 into several steps. Here is a brief overview of what is to come, with some commentary.

First, we reduce to the population limit ( $n = \infty$ ), replacing sums by integrals, via concentration of measure. The integrals are then parameterized by geodesic normal coordinates on the manifold. Both of these steps are standard; elseways, our strategy departs from the approach in the literature for the  $\ell_2$  norm. We replace the Gaussian kernel by the 0/1 kernel, so all considerations are local. The domain of integration becomes the intersection of the manifold  $\mathcal{M}$  with the convex body  $\sigma\mathcal{B}$  (for  $\sigma \rightarrow 0$ ). This being a potentially unwieldy domain, we substitute the Taylor series expansion of the exponential map to replace the manifold  $\mathcal{M}$  by first- and second-order approximations around  $\mathbf{p}$ . For the term involving the second fundamental form, we switch to spherical coordinates. Then, we study the radial domain of integration. This step (Subsection 3.7) comprises the most technical of the proof. Following this, the tilt function emerges (Proposition 3), and dominated convergence is used to finish.

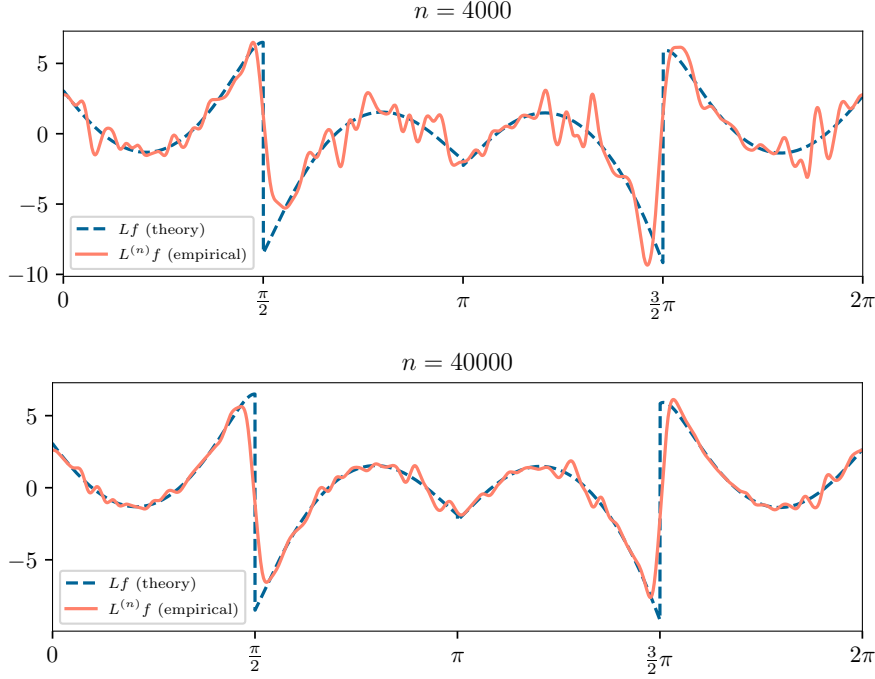


**Fig. 2** Empirical vs. theoretical weighted  $\ell_1$  Laplacian on the circle ( $w_1 = 1, w_2 = 1.5$ ) applied to the function  $f(\theta) = \sin(\theta) + \cos(2\theta) + \cos(5\theta)$ . For the empirical Laplacian, the samples were drawn uniformly at random from the unit circle. (top panel)  $n = 4,000$  samples; (bottom panel)  $n = 40,000$  samples.

### 3.1 Step 1: reduce to the population limit ( $n \rightarrow \infty$ )

This is a standard application of concentration of measure. Set

$$S_n^{(i)} := \text{vol}(\mathcal{M})(C_n/n)K_{\sigma_n}(\|\mathbf{x}^{(i)} - \mathbf{p}\|)(f(\mathbf{x}^{(i)}) - f(\mathbf{p})), \quad S_n := \sum_{i=1}^n S_n^{(i)}. \quad (64)$$

For fixed  $n$ ,  $S_n^{(i)}$  ( $i = 1, \dots, n$ ) are i.i.d. random variables. By continuity of  $f$  and compactness of  $\mathcal{M}$ , there is a constant  $c_0 > 0$  such that  $|f(\mathbf{x})| \leq c_0$  for all  $\mathbf{x} \in \mathcal{M}$ . Then  $S_n^{(i)}$  is bounded,

$$|S_n^{(i)}| \leq (2c_0 \text{vol}(\mathcal{M})C_n)/n. \quad (65)$$

Let  $\epsilon > 0$ . By (65) together with Hoeffding's inequality,

$$\mathbb{P}\left(|S_n - \mathbb{E}[S_n]| \geq \frac{\epsilon}{2}\right) \leq 2\exp\left(\frac{-\epsilon^2 n}{32c_0^2 \text{vol}(\mathcal{M})^2 C_n^2}\right) = 2\exp\left(\frac{-\epsilon^2 \Gamma(\frac{d+4}{2})n^{\frac{\alpha}{2d+4+\alpha}}}{32c_0^2 \text{vol}(\mathcal{M})^2}\right), \quad (66)$$



where we substituted  $C_n = \Gamma(\frac{d+4}{2})^{-1} \sigma_n^{-(d+2)}$  and  $\sigma_n = n^{-1/(2d+4+\alpha)}$ . Here

$$\mathbb{E}[S_n] = \frac{1}{\Gamma(\frac{d+4}{2}) \sigma_n^{d+2}} \int_{\mathbf{x} \in \mathcal{M}} K_{\sigma_n}(\|\mathbf{x} - \mathbf{p}\|) (f(\mathbf{x}) - f(\mathbf{p})) d\mu(\mathbf{x}), \quad (67)$$

where  $d\mu$  is the Riemannian volume density on  $\mathcal{M}$ . Since  $\sigma_n \rightarrow 0$  as  $n \rightarrow \infty$ , assuming we proved

$$\lim_{\sigma \rightarrow 0} \frac{1}{\Gamma(\frac{d+4}{2}) \sigma^{d+2}} \int_{\mathbf{x} \in \mathcal{M}} K_{\sigma}(\|\mathbf{x} - \mathbf{p}\|) (f(\mathbf{x}) - f(\mathbf{p})) d\mu(\mathbf{x}) = \mathcal{L}_{\mathcal{M}, \|\cdot\|} f(\mathbf{p}), \quad (68)$$

then there would exist  $n_0 = n_0(\epsilon)$  such that for all  $n > n_0$ ,

$$|\mathbb{E}[S_n] - \mathcal{L}_{\mathcal{M}, \|\cdot\|}(f)(\mathbf{p})| \leq \frac{\epsilon}{2}. \quad (69)$$

Combining (66) and (69) gives, for all  $n > n_0$ ,

$$\mathbb{P}(|S_n - \mathcal{L}_{\mathcal{M}, \|\cdot\|}(f)(\mathbf{p})| \geq \epsilon) \leq \mathbb{P}(|S_n - \mathbb{E}[S_n]| \geq \frac{\epsilon}{2}) \leq 2 \exp\left(\frac{-\epsilon^2 \Gamma(\frac{d+4}{2}) n^{\frac{\alpha}{2d+4+\alpha}}}{32 c_0^2 \text{vol}(\mathcal{M})^2}\right). \quad (70)$$

By  $\alpha > 0$ , the RHS of (70) converges to 0 as  $n \rightarrow \infty$ . Since  $\epsilon$  was arbitrary, this shows that  $S_n$  converges to  $\mathcal{L}_{\mathcal{M}, \|\cdot\|}(f)(\mathbf{p})$  in probability. It remains to actually prove (68).

### 3.2 Step 2: reduce to the indicator function kernel

In this step, we replace the Gaussian kernel  $K_{\sigma_n}$  by the indicator function kernel  $\mathbb{1}_{\sigma_n}$ ,

$$\mathbb{1}_{\sigma_n} : \mathbb{R}_{\geq 0} \rightarrow \mathbb{R}_{\geq 0} \text{ where } \mathbb{1}_{\sigma_n}(t) := 1 \text{ if } t \in [0, \sigma_n] \text{ and } \mathbb{1}_{\sigma_n}(t) := 0 \text{ if } t > \sigma_n. \quad (71)$$

Precisely, we show

$$\lim_{\sigma \rightarrow 0} \frac{1}{\sigma^{d+2}} \int_{\mathbf{x} \in \mathcal{M}} \mathbb{1}_{\sigma}(\|\mathbf{x} - \mathbf{p}\|) (f(\mathbf{x}) - f(\mathbf{p})) d\mu(\mathbf{x}) = \mathcal{L}_{\mathcal{M}, \|\cdot\|}(f)(\mathbf{p}) \quad (72)$$

implies (68). So, we reduce to proving (72).

To achieve this reduction, let us assume (72). The main point is to write  $K_{\sigma}$  as a sum of indicator functions:

$$K_{\sigma}(t) = \int_{s=0}^{\infty} \kappa_{\sigma}(s) \mathbb{1}_s(t) ds = \int_{s=t}^{\infty} \kappa_{\sigma}(s) ds, \quad (73)$$

where  $\kappa_\sigma : \mathbb{R}_{\geq 0} \rightarrow \mathbb{R}_{\geq 0}$  is given by  $\kappa_\sigma(s) := (2s/\sigma^2)\exp(-s^2/\sigma^2)$ . Then,

$$\begin{aligned}
& \int_{\mathbf{x} \in \mathcal{M}} K_\sigma(\|\mathbf{x} - \mathbf{p}\|)(f(\mathbf{x}) - f(\mathbf{p}))d\mu(\mathbf{x}) \\
&= \int_{\mathbf{x} \in \mathcal{M}} \left( \int_{s=\|\mathbf{x}-\mathbf{p}\|}^{\infty} \kappa_\sigma(s)ds \right) (f(\mathbf{x}) - f(\mathbf{p}))d\mu(\mathbf{x}) \quad [\text{substituting (73)}] \\
&= \int_{s=0}^{\infty} \kappa_\sigma(s) \left( \int_{\mathbf{x} \in \mathcal{M}: \|\mathbf{x}-\mathbf{p}\| \leq s} f(\mathbf{x}) - f(\mathbf{p})d\mu(\mathbf{x}) \right) ds \quad [\text{Fubini's theorem}].
\end{aligned} \tag{74}$$

Define

$$e(s) := \left( \int_{\mathbf{x} \in \mathcal{M}: \|\mathbf{x}-\mathbf{p}\| \leq s} f(\mathbf{x}) - f(\mathbf{p})d\mu(\mathbf{x}) \right) - s^{d+2} \mathcal{L}_{\mathcal{M}, \|\cdot\|}(f)(\mathbf{p}). \tag{75}$$

Assuming (72),

$$e(s) = o(s^{d+2}) \text{ as } s \rightarrow 0. \tag{76}$$

Fix  $\epsilon > 0$ . By (76), we can fix  $\delta > 0$  so

$$0 \leq s \leq \delta \Rightarrow |e(s)| \leq \epsilon s^{d+2}. \tag{77}$$

Returning to (74),

$$\begin{aligned}
& \int_{s=0}^{\infty} \kappa_\sigma(s) \left( \int_{\mathbf{x} \in \mathcal{M}: \|\mathbf{x}-\mathbf{p}\| \leq s} f(\mathbf{x}) - f(\mathbf{p})d\mu(\mathbf{x}) \right) ds \\
&=: \int_{s=0}^{\delta} \kappa_\sigma(s) \left( \int_{\mathbf{x} \in \mathcal{M}: \|\mathbf{x}-\mathbf{p}\| \leq s} f(\mathbf{x}) - f(\mathbf{p})d\mu(\mathbf{x}) \right) ds + \exp(-\delta^2/\sigma^2)\text{poly}(\sigma).
\end{aligned} \tag{78}$$

To see (78), note the parenthesized integral has absolute value bounded by  $2c_0 \text{vol}(\mathcal{M})$  for all  $s \in [0, \infty]$ , by compactness of  $\mathcal{M}$ . So, an easy tail bound for the Gaussian gives (78) (put  $k = 0$  in Equation (169) in Appendix B).

Now the main term in (78) is

$$\int_{s=0}^{\delta} \kappa_\sigma(s) (s^{d+2} \mathcal{L}_{\mathcal{M}, \|\cdot\|}(f)(\mathbf{p}) + e(s)) ds. \tag{79}$$

From (77), this is bounded above by

$$\int_{s=0}^{\delta} \kappa_\sigma(s) s^{d+2} (\mathcal{L}_{\mathcal{M}, \|\cdot\|}(f)(\mathbf{p}) + \epsilon) ds, \tag{80}$$

and below by

$$\int_{s=0}^{\delta} \kappa_\sigma(s) s^{d+2} (\mathcal{L}_{\mathcal{M}, \|\cdot\|}(f)(\mathbf{p}) - \epsilon) ds. \tag{81}$$

By more easy bounds for the Gaussian (Appendix B), (80) and (81) equal

$$\int_{s=0}^{\infty} \kappa_{\sigma}(s) s^{d+2} (\mathcal{L}_{\mathcal{M}, \|\cdot\|}(f)(\mathbf{p}) \pm \epsilon) ds + \exp(-\delta^2/\sigma^2) \text{poly}(\sigma). \quad (82)$$

But, the main term is

$$\sigma^{d+2} \Gamma(\frac{d+4}{2}) (\mathcal{L}_{\mathcal{M}, \|\cdot\|}(f)(\mathbf{p}) \pm \epsilon), \quad (83)$$

by the formula for half the  $k$ -th absolute moment of  $\kappa_{\sigma}$  ((171) in Appendix B). Using  $\lim_{\sigma \rightarrow 0} \exp(-\delta^2/\sigma^2) \text{poly}(\sigma) = 0$ , and the fact that  $\epsilon$  was arbitrary,

$$\int_{\mathbf{x} \in \mathcal{M}} \lim_{\sigma \rightarrow 0} \frac{1}{\sigma^{d+2}} K_{\sigma}(\|\mathbf{x} - \mathbf{p}\|) (f(\mathbf{x}) - f(\mathbf{p})) d\mu(\mathbf{x}) = \Gamma(\frac{d+4}{2}) \mathcal{L}_{\mathcal{M}, \|\cdot\|}(f)(\mathbf{p}). \quad (84)$$

Therefore, (72) implies (68). We have reduced to proving the limit with indicator functions (72).

### 3.3 Step 3: use geodesic normal coordinates and Taylor expand

In this step, we set up the integral in the LHS of (72),

$$\int_{\mathbf{x} \in \mathcal{M}: \|\mathbf{x} - \mathbf{p}\| \leq \sigma} f(\mathbf{x}) - f(\mathbf{p}) d\mu(\mathbf{x}). \quad (85)$$

We parameterize this using the exponential map (Subsection 2.1),

$$\exp_{\mathbf{p}} : U \xrightarrow{\sim} V, \quad (86)$$

where  $U \subseteq T_{\mathbf{p}}\mathcal{M}$  and  $V \subseteq \mathcal{M}$  are open neighborhoods of 0 and  $\mathbf{p}$  and  $\mathbf{s} = (s_1, \dots, s_d)^{\top}$  are coordinates for  $T_{\mathbf{p}}\mathcal{M}$  with respect to an orthonormal basis. Note there is  $\sigma_0 > 0$  such that for  $\sigma \leq \sigma_0$  the domain of integration in (72) is contained in  $V$ ,

$$\{\mathbf{x} \in \mathcal{M} : \|\mathbf{x} - \mathbf{p}\| \leq \sigma\} \subseteq V, \quad (87)$$

by definition of  $\mathcal{M}$  being an embedded submanifold of  $\mathbb{R}^D$ . Then, for  $\sigma \leq \sigma_0$ , change of variables says (85) equals

$$\int_{\mathbf{s} \in U: \|\exp_{\mathbf{p}}(\mathbf{s}) - \mathbf{p}\| \leq \sigma} (\tilde{f}(\mathbf{s}) - \tilde{f}(0)) |\det D\exp_{\mathbf{p}}(\mathbf{s})| d\mathbf{s}, \quad (88)$$

where  $d\mathbf{s}$  is the Lebesgue measure on  $(T_{\mathbf{p}}\mathcal{M}, \langle \cdot, \cdot \rangle_{\mathbf{p}})$ .

We want (88) to order  $\sigma^{d+2}$ . For this, we consider three Taylor expansions:

$$\tilde{f}(\mathbf{s}) = \tilde{f}(0) + \nabla \tilde{f}(0)^{\top} \mathbf{s} + \frac{1}{2} \mathbf{s}^{\top} \nabla^2 \tilde{f}(0) \mathbf{s} + O(\|\mathbf{s}\|_2^3), \quad (89)$$

$$\det D\exp_{\mathbf{p}}(\mathbf{s}) = 1 - \frac{1}{6} \mathbf{s}^{\top} \text{Ric}(\mathbf{p}) \mathbf{s} + O(\|\mathbf{s}\|_2^3) = 1 + O(\|\mathbf{s}\|_2^2), \quad (90)$$

$$\exp_{\mathbf{p}}(\mathbf{s}) = \mathbf{p} + L_{\mathbf{p}}(\mathbf{s}) + \frac{1}{2} Q_{\mathbf{p}}(\mathbf{s}) + O(\|\mathbf{s}\|_2^3). \quad (91)$$

Here,  $\text{Ric}(\mathbf{p}) \in \mathbb{R}^{d \times d}$  stands for the *Ricci curvature* of  $\mathcal{M}$  at  $\mathbf{p}$  (see [34, Chapter 7]). Also, see Subsection 2.1 for discussion on  $L_{\mathbf{p}}$  and  $Q_{\mathbf{p}}$ .

It will be convenient to shrink  $U$  and  $V$  in (87) as necessary so

$$\|\exp_{\mathbf{p}}(\mathbf{s}) - \mathbf{p} - L_{\mathbf{p}}(\mathbf{s})\| \leq \frac{1}{2}\|\mathbf{s}\|_2 \quad \text{for all } \mathbf{s} \in U. \quad (92)$$

At this point, substituting (89) and (90) into (88), gives us the crucial integral

$$\int_{\mathbf{s} \in U: \|\exp_{\mathbf{p}}(\mathbf{s}) - \mathbf{p}\| \leq \sigma} \nabla \tilde{f}(0)^\top \mathbf{s} + \frac{1}{2} \mathbf{s}^\top \nabla^2 \tilde{f}(0) \mathbf{s} + O(\|\mathbf{s}\|_2^3) d\mathbf{s}. \quad (93)$$

### 3.4 Step 4: approximate the domain of integration

In this step, we approximate the domain of integration in (93) using the Taylor expansion of the exponential map (Definition 3). Then we assess the quality of our approximations (Proposition 1).

**Definition 3** For each  $\sigma$ , define three subsets of  $T_{\mathbf{p}}\mathcal{M}$ :

$$\text{Exact}_U(\sigma) := \{\mathbf{s} \in U : \|\exp_{\mathbf{p}}(\mathbf{s}) - \mathbf{p}\| \leq \sigma\}, \quad (94)$$

$$\text{Approx}_1(\sigma) := \{\mathbf{s} \in T_{\mathbf{p}}\mathcal{M} : \|L_{\mathbf{p}}(\mathbf{s})\| \leq \sigma\}, \quad (95)$$

$$\text{Approx}_2(\sigma) := \{\mathbf{s} \in T_{\mathbf{p}}\mathcal{M} : \|L_{\mathbf{p}}(\mathbf{s}) + \frac{1}{2}Q_{\mathbf{p}}(\mathbf{s})\| \leq \sigma\}. \quad (96)$$

**Proposition 1** *i. There exist constants  $c_1, \sigma_1 > 0$  such that for all  $\sigma \leq \sigma_1$ ,*

$$\text{Exact}_U(\sigma) \subseteq c_1 \{\mathbf{s} \in T_{\mathbf{p}}\mathcal{M} : \|\mathbf{s}\|_2 \leq \sigma\}. \quad (97)$$

*ii. There exist constants  $c_2, c_3, \sigma_2 > 0$  such that for all  $\sigma \leq \sigma_2$ ,*

$$(1 - c_3\sigma)\text{Approx}_1(\sigma) \subseteq \text{Exact}_U(\sigma) \subseteq (1 + c_2\sigma)\text{Approx}_1(\sigma). \quad (98)$$

*iii. There exist constants  $c_4, c_5, \sigma_3 > 0$  such that for all  $\sigma \leq \sigma_3$ ,*

$$(1 - c_5\sigma^2)\text{Approx}_2(\sigma) \subseteq \text{Exact}_U(\sigma) \subseteq (1 + c_4\sigma^2)\text{Approx}_2(\sigma). \quad (99)$$

*Proof* part i. Let  $\mathbf{s} \in \text{Exact}_U(\sigma)$ . From the equivalence of norms on  $\mathbb{R}^D$  (18), assumption (92), the triangle inequality and isometry property (14),

$$\begin{aligned} \sigma \geq \|\exp_{\mathbf{p}}(\mathbf{s}) - \mathbf{p}\| &\gtrsim \|L_{\mathbf{p}}(\mathbf{s}) + (\exp_{\mathbf{p}}(\mathbf{s}) - \mathbf{p} - L_{\mathbf{p}}(\mathbf{s}))\|_2 \\ &\geq \|L_{\mathbf{p}}(\mathbf{s})\|_2 - \frac{1}{2}\|\mathbf{s}\|_2 = \frac{1}{2}\|\mathbf{s}\|_2. \end{aligned} \quad (100)$$

Hence,  $\|\mathbf{s}\|_2 = O(\sigma)$ .

part ii. For the rightmost inclusion, assume  $\mathbf{s} \in \text{Exact}_U(\sigma)$ , so

$$\sigma \geq \|\exp_{\mathbf{p}}(\mathbf{s}) - \mathbf{p}\| = \|L_{\mathbf{p}}(\mathbf{s}) + O(\|\mathbf{s}\|_2^2)\|. \quad (101)$$

By the triangle inequality and part i,

$$\|L_{\mathbf{p}}(\mathbf{s})\| \leq \sigma + O(\|\mathbf{s}\|_2^2) = \sigma + O(\sigma^2). \quad (102)$$

Thus, take  $c_2$  to be the implicit constant in  $O(\sigma^2)$  in (102).

For the leftmost inclusion, observe by the triangle inequality, isometry property (14), and equivalence of norms (18):

$$\begin{aligned} \|\exp_{\mathbf{p}}(\mathbf{s}) - \mathbf{p}\| &\leq \|L_{\mathbf{p}}(\mathbf{s})\| + O(\|\mathbf{s}\|_2^2) = \|L_{\mathbf{p}}(\mathbf{s})\| + O(\|L_{\mathbf{p}}(\mathbf{s})\|_2^2) \\ &\leq \|L_{\mathbf{p}}(\mathbf{s})\| + O(\|L_{\mathbf{p}}(\mathbf{s})\|^2). \end{aligned} \quad (103)$$

Let  $c_3 > 0$  be the constant implicit in the last big  $O$  of (103). Assume  $\mathbf{s}$  satisfies  $\|L_{\mathbf{p}}(\mathbf{s})\| \leq \sigma - c_3\sigma^2$ . Substituting into (103),

$$\|\exp_{\mathbf{p}}(\mathbf{s}) - \mathbf{p}\| \leq (\sigma - c_3\sigma^2) + c_3(\sigma - c_3\sigma^2)^2 = \sigma - 2c_3^3\sigma^3 + O(\sigma^4) \leq \sigma, \quad (104)$$

where the inequalities hold for all sufficiently small  $\sigma$ .

part iii. For the rightmost inclusion, assume  $\mathbf{s} \in \text{Exact}_U(\sigma)$ , so

$$\sigma \geq \|\exp_{\mathbf{p}}(\mathbf{s}) - \mathbf{p}\| = \|L_{\mathbf{p}}(\mathbf{s}) + \tfrac{1}{2}Q_{\mathbf{p}}(\mathbf{s}) + O(\|\mathbf{s}\|_2^3)\|. \quad (105)$$

By part i,  $\|\mathbf{s}\|_2 = O(\sigma)$ . From (105) and the triangle inequality,

$$\|L_{\mathbf{p}}(\mathbf{s}) + \tfrac{1}{2}Q_{\mathbf{p}}(\mathbf{s})\| \leq \sigma + c'_4\sigma^3, \quad (106)$$

for some constant  $c'_4 > 0$  and all sufficiently small  $\sigma$ . We want to find to a constant  $c_4 > 0$  such that  $\mathbf{s}/(1 + c_4\sigma^2) \in \text{Approx}_2(\sigma)$ . To this end, compute

$$\begin{aligned} &\left\| \frac{1}{1 + c_4\sigma^2} L_{\mathbf{p}}(\mathbf{s}) + \frac{1}{(1 + c_4\sigma^2)^2} \frac{1}{2} Q_{\mathbf{p}}(\mathbf{s}) \right\| \\ &\leq \frac{1}{1 + c_4\sigma^2} \|L_{\mathbf{p}}(\mathbf{s}) + \tfrac{1}{2}Q_{\mathbf{p}}(\mathbf{s})\| + \left( \frac{1}{1 + c_4\sigma^2} - \frac{1}{(1 + c_4\sigma^2)^2} \right) \|\tfrac{1}{2}Q_{\mathbf{p}}(\mathbf{s})\| \\ &\leq \frac{1}{1 + c_4\sigma^2} (\sigma + c'_4\sigma^3) + \left( \frac{1}{1 + c_4\sigma^2} - \frac{1}{(1 + c_4\sigma^2)^2} \right) O(\sigma^2) \\ &= (1 - c_4\sigma^2 + O(\sigma^4)) (\sigma + c'_4\sigma^3) + (c_4\sigma^2 + O(\sigma^4)) O(\sigma^2) \\ &= \sigma + (c'_4 - c_4)\sigma^3 + O(\sigma^4). \end{aligned} \quad (107)$$

Here we used the triangle inequality, the bound (106), part i, and Taylor expansions in  $\sigma$  for  $(1 + c_4\sigma^2)^{-1}$  and  $(1 + c_4\sigma^2)^{-2}$ . Thus, take  $c_4 = 2c'_4$ . For small enough  $\sigma$ , the RHS of (107) is at most  $\sigma$ , so  $\mathbf{s}/(1 + c_4\sigma^2) \in \text{Approx}_2(\sigma)$ .

Now consider the leftmost inclusion in part iii. Assume  $\mathbf{s} \in \text{Approx}_2(\sigma)$ . We first prove that  $\|\mathbf{s}\|_2 = O(\sigma)$ . Indeed,

$$\begin{aligned} \sigma &\geq \|L_{\mathbf{p}}(\mathbf{s}) + \tfrac{1}{2}Q_{\mathbf{p}}(\mathbf{s})\| \gtrsim \|L_{\mathbf{p}}(\mathbf{s}) + \tfrac{1}{2}Q_{\mathbf{p}}(\mathbf{s})\|_2 \\ &= \sqrt{\|L_{\mathbf{p}}(\mathbf{s})\|_2^2 + \tfrac{1}{4}\|Q_{\mathbf{p}}(\mathbf{s})\|_2^2} \geq \|L_{\mathbf{p}}(\mathbf{s})\|_2 = \|\mathbf{s}\|_2. \end{aligned} \quad (108)$$

The first equality comes from orthogonality between the images of  $Q_{\mathbf{p}}$  and  $L_{\mathbf{p}}$  (15). Let the implicit constant in (108) be  $c'_5$ . Similarly to above, let us set  $c_5 = 2c'_5$  and compute (for sufficiently small  $\sigma$ ):

$$\begin{aligned} \|\exp_{\mathbf{p}}((1 - c_5\sigma^2)\mathbf{s}) - \mathbf{p}\| &\leq \|(1 - c_5\sigma^2)L_{\mathbf{p}}(\mathbf{s}) + (1 - c_5\sigma^2)^2 \frac{1}{2}Q_{\mathbf{p}}(\mathbf{s})\| + c'_5\sigma^3 \\ &\leq (1 - c_5\sigma^2)\|L_{\mathbf{p}} + \frac{1}{2}Q_{\mathbf{p}}(\mathbf{s})\| + ((1 - c_5\sigma^2) - (1 - c_5\sigma^2)^2)\|\frac{1}{2}Q_{\mathbf{p}}(\mathbf{s})\| + c'_5\sigma^3 \\ &\leq (1 - c_5\sigma^2)\sigma + O(\sigma^4) + c'_5\sigma^3 = \sigma - c'_5\sigma^3 + O(\sigma^4) \leq \sigma. \end{aligned} \quad (109)$$

We used the Taylor expansion (91), the triangle inequality, the bound (108), and the triangle inequality again. So,  $(1 - c_5\sigma^2)\mathbf{s} \in \text{Exact}_U(\sigma)$ . This completes the proof of Proposition 1.  $\square$

### 3.5 Step 5: drop $O(\|\mathbf{s}\|_2^3)$ and obtain the second-order term

Return to the integral (93). With Proposition 1, we examine each term in turn.

**Proposition 2** *The following bounds hold:*

i.

$$\int_{\mathbf{s} \in \text{Exact}_U(\sigma)} O(\|\mathbf{s}\|_2^3) d\mathbf{s} = O(\sigma^{d+3}), \quad (110)$$

ii.

$$\int_{\mathbf{s} \in \text{Exact}_U(\sigma)} \mathbf{s}\mathbf{s}^\top d\mathbf{s} = \int_{\mathbf{s} \in \text{Approx}_1(\sigma)} \mathbf{s}\mathbf{s}^\top d\mathbf{s} + O(\sigma^{d+3}), \quad (111)$$

iii.

$$\int_{\mathbf{s} \in \text{Exact}_U(\sigma)} \mathbf{s} d\mathbf{s} = \int_{\mathbf{s} \in \text{Approx}_2(\sigma)} \mathbf{s} d\mathbf{s} + O(\sigma^{d+3}). \quad (112)$$

*Proof* Let  $\triangle$  denote the symmetric difference of sets.

part i. Let  $\sigma \leq \sigma_1$ . By Proposition 1 (part i),

$$\begin{aligned} \int_{\mathbf{s} \in \text{Exact}_U(\sigma)} O(\|\mathbf{s}\|_2^3) d\mathbf{s} &\lesssim \int_{\|\mathbf{s}\|_2 \leq c_2\sigma} \|\mathbf{s}\|_2^3 \leq \int_{\|\mathbf{s}\|_\infty \leq c_2\sigma} \|\mathbf{s}\|_2^3 d\mathbf{s} \\ &\lesssim \int_{\|\mathbf{s}\|_\infty \leq c_2\sigma} \|\mathbf{s}\|_3^3 d\mathbf{s} = d2^{d-2}c_2^{d+3}\sigma^{d+3} = O(\sigma^{d+3}). \end{aligned} \quad (113)$$

part ii. Let  $\sigma \leq \sigma_2$ . By Proposition 1 (part ii),

$$\text{Exact}_U(\sigma) \triangle \text{Approx}_1(\sigma) \subseteq (1 + c_2\sigma)\text{Approx}_1(\sigma) \setminus (1 - c_3\sigma)\text{Approx}_1(\sigma). \quad (114)$$

Then,

$$\begin{aligned}
& \left\| \int_{\mathbf{s} \in \text{Exact}_U(\sigma)} \mathbf{s} \mathbf{s}^\top d\mathbf{s} - \int_{\mathbf{s} \in \text{Approx}_1(\sigma)} \mathbf{s} \mathbf{s}^\top d\mathbf{s} \right\|_F \\
& \leq \int_{\mathbf{s} \in \text{Exact}_U(\sigma) \triangle \text{Approx}_1(\sigma)} \|\mathbf{s} \mathbf{s}^\top\|_F d\mathbf{s} \\
& \leq \int_{\mathbf{s} \in (1+c_2\sigma)\text{Approx}_1(\sigma) \setminus (1-c_3\sigma)\text{Approx}_1(\sigma)} \|\mathbf{s}\|_2^2 d\mathbf{s} \\
& = ((\sigma + c_3\sigma^2)^{d+2} - (\sigma - c_2\sigma^2)^{d+2}) \int_{\|L_{\mathbf{P}}(\mathbf{s})\| \leq 1} \|\mathbf{s}\|_2^2 d\mathbf{s} \\
& = O(\sigma^{d+3}) \int_{\|\mathbf{s}\|_\infty \leq O(1)} \|\mathbf{s}\|_2^2 d\mathbf{s} \\
& = O(\sigma^{d+3}).
\end{aligned} \tag{115}$$

Here the first equality is by change of variables (linear scaling), and the second equality comes from  $\|\mathbf{s}\|_\infty \lesssim \|\mathbf{s}\|_2 = \|L_{\mathbf{P}}(\mathbf{s})\|_2 \lesssim \|L_{\mathbf{P}}(\mathbf{s})\|_\infty$ .

part iii. Let  $\sigma \leq \sigma_3$ . By Proposition 1 (part iii),

$$\text{Exact}_U(\sigma) \triangle \text{Approx}_2(\sigma) \subseteq (1 + c_4\sigma^2)\text{Approx}_2(\sigma) \setminus (1 - c_5\sigma^2)\text{Approx}_2(\sigma). \tag{116}$$

Then,

$$\begin{aligned}
& \left\| \int_{\mathbf{s} \in \text{Exact}_U(\sigma)} \mathbf{s} d\mathbf{s} - \int_{\mathbf{s} \in \text{Approx}_2(\sigma)} \mathbf{s} d\mathbf{s} \right\|_2 \\
& \leq \int_{\mathbf{s} \in \text{Exact}_U(\sigma) \triangle \text{Approx}_2(\sigma)} \|\mathbf{s}\|_2 d\mathbf{s} \\
& \leq \int_{\mathbf{s} \in (1+c_4\sigma^2)\text{Approx}_2(\sigma) \setminus (1-c_5\sigma^2)\text{Approx}_2(\sigma)} \|\mathbf{s}\|_2 d\mathbf{s} \\
& = ((1 + c_4\sigma^2)^{d+1} - (1 - c_5\sigma^2)^{d+1}) \int_{\mathbf{s} \in \text{Approx}_2(\sigma)} \|\mathbf{s}\|_2 d\mathbf{s} \\
& = O(\sigma^2) \int_{\|\mathbf{s}\|_2 \leq O(1)} \|\mathbf{s}\|_2 d\mathbf{s} \\
& = O(\sigma^2) \int_{\|\mathbf{s}\|_\infty \leq O(1)} \|\mathbf{s}\|_1 d\mathbf{s} \\
& = O(\sigma^{d+3}).
\end{aligned} \tag{117}$$

The first equality is by linear scaling. The second is because  $\mathbf{s} \in \text{Approx}_2(\sigma)$  implies  $\|\mathbf{s}\|_2 = O(\sigma)$ , as established in the proof of Proposition 1 (part iii). This completes the proof of Proposition 2.  $\square$

Now, plug Proposition 2 into (93):

$$\begin{aligned} & \int_{\mathbf{s} \in U: \|\exp_{\mathbf{p}}(\mathbf{s}) - \mathbf{p}\| \leq \sigma} \nabla \tilde{f}(0)^\top \mathbf{s} + \frac{1}{2} \mathbf{s}^\top \nabla^2 \tilde{f}(0) \mathbf{s} + O(\|\mathbf{s}\|_2^3) d\mathbf{s} \\ &= \left\langle \nabla \tilde{f}(0), \int_{\mathbf{s} \in \text{Approx}_2(\sigma)} \mathbf{s} d\mathbf{s} \right\rangle + \left\langle \nabla^2 \tilde{f}(0), \frac{1}{2} \int_{\mathbf{s} \in \text{Approx}_1(\sigma)} \mathbf{s} \mathbf{s}^\top d\mathbf{s} \right\rangle + O(\sigma^{d+3}), \end{aligned} \quad (118)$$

where linearity of  $L_{\mathbf{p}}$  gives

$$\int_{\mathbf{s} \in \text{Approx}_1(\sigma)} \mathbf{s} \mathbf{s}^\top d\mathbf{s} = \sigma^{d+2} \int_{\mathbf{s}: \|L_{\mathbf{p}}(\mathbf{s})\| \leq 1} \mathbf{s} \mathbf{s}^\top d\mathbf{s}. \quad (119)$$

Thus, (93) divided by  $\sigma^{d+2}$  tends to  $\mathcal{L}_{\mathcal{M}, \|\cdot\|}(f)(\mathbf{p})$  as  $\sigma \rightarrow 0$ , as desired, provided we can show

$$\lim_{\sigma \rightarrow 0} \frac{1}{\sigma^{d+2}} \int_{\mathbf{s} \in \text{Approx}_2(\sigma)} \mathbf{s} d\mathbf{s} = \int_{\|\hat{\mathbf{s}}\|_2=1} \hat{\mathbf{s}} \|L_{\mathbf{p}}(\hat{\mathbf{s}})\|^{-d} \text{tilt}_{\mathcal{M}, \mathcal{B}, \mathbf{p}}(\hat{\mathbf{s}}) d\hat{\mathbf{s}}. \quad (120)$$

### 3.6 Step 6: use spherical coordinates

It remains to estimate

$$\int_{\mathbf{s}: \|L_{\mathbf{p}}(\mathbf{s}) + \frac{1}{2} Q_{\mathbf{p}}(\mathbf{s})\| \leq \sigma} \mathbf{s} d\mathbf{s}. \quad (121)$$

First, we provide intuition for this might be  $O(\sigma^{d+2})$  at all. Let  $\mathbb{S}^{d-1} \subseteq \mathbb{R}^d \cong T_{\mathbf{p}}\mathcal{M}$  denote the  $\ell_2$ -unit sphere, with density  $d\hat{\mathbf{s}}$ , where  $\hat{\mathbf{s}} \in \mathbb{S}^{d-1}$ . Let  $r \in \mathbb{R}_{\geq 0}$  be a radial variable with density  $dr$ . Consider (121) in these spherical coordinates. Substituting  $\mathbf{s} = r\hat{\mathbf{s}}$  and  $d\mathbf{s} = r^{d-1} dr d\hat{\mathbf{s}}$ ,

$$\int_{\mathbf{s}: \|L_{\mathbf{p}}(\mathbf{s}) + \frac{1}{2} Q_{\mathbf{p}}(\mathbf{s})\| \leq \sigma} \mathbf{s} d\mathbf{s} = \int_{\hat{\mathbf{s}} \in \mathbb{S}^{d-1}} \hat{\mathbf{s}} \int_{r \in \text{RadialDomain}(\hat{\mathbf{s}}, \sigma)} r^d dr d\hat{\mathbf{s}}, \quad (122)$$

where we define

$$\text{RadialDomain}(\hat{\mathbf{s}}, \sigma) := \{r \geq 0 : \|rL_{\mathbf{p}}(\hat{\mathbf{s}}) + r^2 \frac{1}{2} Q_{\mathbf{p}}(\hat{\mathbf{s}})\| \leq \sigma\}. \quad (123)$$

Compare this domain of integration against the domain for  $-\hat{\mathbf{s}}$ :

$$\begin{aligned} \text{RadialDomain}(-\hat{\mathbf{s}}, \sigma) &= \{r \geq 0 : \|rL_{\mathbf{p}}(-\hat{\mathbf{s}}) + r^2 \frac{1}{2} Q_{\mathbf{p}}(-\hat{\mathbf{s}})\| \leq \sigma\} \\ &= \{r \geq 0 : \|rL_{\mathbf{p}}(\hat{\mathbf{s}}) - r^2 \frac{1}{2} Q_{\mathbf{p}}(\hat{\mathbf{s}})\| \leq \sigma\}. \end{aligned} \quad (124)$$

Speaking roughly, the condition determining membership in (123) differs from that in (124) at the  $O(r^2)$  term; the conditions would be the same without the  $Q_{\mathbf{p}}$  term. On the other hand, the integrand in (122) is odd (that is, it flips sign



upon inversion in the origin). Therefore, we should expect “near cancellation” between the inner integrals:

$$\widehat{\mathbf{s}} \int_{r \in \text{RadialDomain}(\widehat{\mathbf{s}}, \sigma)} r^d dr - \widehat{\mathbf{s}} \int_{r \in \text{RadialDomain}(-\widehat{\mathbf{s}}, \sigma)} r^d dr. \quad (125)$$

Supposing  $r = O(\sigma)$  for  $r$  in each radial domain (justified in Lemma 2), then each of the two terms in (125) is  $O(\sigma^{d+1})$ . Thus after “near, but not complete, cancellation” the sum (125) is expected to be  $O(\sigma^{d+2})$ . Then, integrating over the unit sphere gives  $O(\sigma^{d+2})$  in (122).

This informal discussion explains why we anticipate (121) to be  $O(\sigma^{d+2})$ , the mechanism being cancellation due to an approximate equality between  $\text{RadialDomain}(\widehat{\mathbf{s}}, \sigma)$  and  $\text{RadialDomain}(-\widehat{\mathbf{s}}, \sigma)$ .

We shall succeed in making this approach rigorous. Beyond proving (122) is  $O(\sigma^{d+2})$ , we will prove (122) divided by  $\sigma^{d+2}$  has a well-defined limit, the RHS of (120). The detailed reasoning (steps 3.7 and 3.8) is complicated by the fact we do not assume smoothness of the norm  $\|\cdot\|$ . E.g., this precludes *a priori* consideration of a Taylor expansion in  $\sigma$  for the boundary points of (123).

**Lemma 2** *There exist constants  $c_6, \sigma_4 > 0$  such that for all  $\sigma \leq \sigma_4$  and all  $\widehat{\mathbf{s}} \in \mathbb{S}^{d-1}$ ,*

$$\text{RadialDomain}(\widehat{\mathbf{s}}, \sigma) \subseteq c_6[0, \sigma]. \quad (126)$$

*Proof* Set  $c_6 := 2c_1$  and  $\sigma_4 := \min\left(\sigma_1, \sigma_3, \frac{1}{\sqrt{2c_5}}\right)$ . For  $\sigma \leq \sigma_4$ ,

$$\text{Approx}_2(\sigma) \subseteq \frac{1}{1 - c_5\sigma^2} \text{Exact}_U(\sigma) \subseteq \frac{c_1}{1 - c_5\sigma^2} \{\mathbf{s} \in \mathbb{R}^d : \|\mathbf{s}\|_2 \leq \sigma\}, \quad (127)$$

by (99) and (97). At the same time,  $\sigma \leq \frac{1}{\sqrt{2c_5}}$  implies  $\frac{c_1}{1 - c_5\sigma^2} \leq 2c_1 = c_6$ . So

$$\text{Approx}_2(\sigma) \subseteq c_6\{\mathbf{s} \in \mathbb{R}^d : \|\mathbf{s}\|_2 \leq \sigma\}, \quad (128)$$

whence  $\text{RadialDomain}(\widehat{\mathbf{s}}, \sigma) \subseteq c_6[0, \sigma]$  for each  $\widehat{\mathbf{s}} \in \mathbb{S}^{d-1}$ .  $\square$

### 3.7 Step 7: study the boundary of $\text{RadialDomain}(\widehat{\mathbf{s}}, \sigma)$

In this step, we show that for small enough  $\sigma$ , the set  $\text{RadialDomain}(\widehat{\mathbf{s}}, \sigma)$  is a single closed interval in  $\mathbb{R}_{\geq 0}$ . Then, we prove its nonzero boundary point is a continuous function of  $(\widehat{\mathbf{s}}, \sigma)$  and we bound this to second-order in  $\sigma$ .

Let  $G : \mathbb{S}^{d-1} \times \mathbb{R}_{\geq 0} \rightarrow \mathbb{R}_{\geq 0}$ ;  $(\widehat{\mathbf{s}}, r) \mapsto \|rL_{\mathbf{p}}(\widehat{\mathbf{s}}) + r^2 \frac{1}{2}Q_{\mathbf{p}}(\widehat{\mathbf{s}})\|$ .

**Lemma 3** *There exists a constant  $c_7 > 0$  such that for each  $\widehat{\mathbf{s}} \in \mathbb{S}^{d-1}$ , the function  $r \mapsto G(\widehat{\mathbf{s}}, r)$  is strictly increasing over  $r \in [0, c_7]$ .*

*Proof* We will show that we can take

$$c_7 := \begin{cases} 1 & \text{if } Q_{\mathbf{p}} \equiv 0, \\ \min_{\widehat{\mathbf{s}} \in \mathbb{S}^{d-1}} \|L_{\mathbf{p}}(\widehat{\mathbf{s}})\| / \max_{\widehat{\mathbf{s}} \in \mathbb{S}^{d-1}} \|Q_{\mathbf{p}}(\widehat{\mathbf{s}})\| & \text{otherwise.} \end{cases} \quad (129)$$

Obviously  $c_7 > 0$ , because  $\|L_{\mathbf{p}}(\widehat{\mathbf{s}})\| \gtrsim \|L_{\mathbf{p}}(\widehat{\mathbf{s}})\|_2 = \|\widehat{\mathbf{s}}\|_2 = 1$  by equivalence of norms and (14), and  $Q_{\mathbf{p}}(\widehat{\mathbf{s}}) = O(1)$  by continuity and compactness.

Fix  $\widehat{\mathbf{s}} \in \mathbb{S}^{d-1}$ . Set  $g : \mathbb{R}_{\geq 0} \rightarrow \mathbb{R}_{\geq 0}$  by  $g(r) = G(\widehat{\mathbf{s}}, r)$ ,  $\mathbf{a} := L_{\mathbf{p}}(\widehat{\mathbf{s}})$  and  $\mathbf{b} := \frac{1}{2}Q_{\mathbf{p}}(\widehat{\mathbf{s}})$ . Since  $g$  is continuous, we may check  $g$  is strictly increasing on the half-open interval  $[0, c_7)$ .

Let  $0 < r < c_7$ . Then,

$$g(r) = \|r\mathbf{a} + r^2\mathbf{b}\| \geq r(\|\mathbf{a}\| - r\|\mathbf{b}\|) > r(\|\mathbf{a}\| - \frac{1}{2}\|\mathbf{a}\|) \geq \frac{r}{2}\|\mathbf{a}\| > 0 = g(0). \quad (130)$$

Let  $\lambda > 0$  be such that  $(1 + \lambda)r < c_7$ , and estimate

$$\begin{aligned} & g((1 + \lambda)r) \\ &= \|r(1 + \lambda)\mathbf{a} + r^2(1 + \lambda)^2\mathbf{b}\| \\ &= \|(1 + \lambda)(r\mathbf{a} + r^2\mathbf{b}) + (\lambda + \lambda^2)r^2\mathbf{b}\| \\ &\geq (1 + \lambda)\|r\mathbf{a} + r^2\mathbf{b}\| - (\lambda + \lambda^2)r^2\|\mathbf{b}\| \\ &= \|r\mathbf{a} + r^2\mathbf{b}\| + \lambda r(\|\mathbf{a} + r\mathbf{b}\| - (1 + \lambda)r\|\mathbf{b}\|) \\ &\geq \|r\mathbf{a} + r^2\mathbf{b}\| + \lambda r(\|\mathbf{a}\| - r\|\mathbf{b}\| - (1 + \lambda)r\|\mathbf{b}\|) \\ &> \|r\mathbf{a} + r^2\mathbf{b}\| + \lambda r(\|\mathbf{a}\| - \frac{1}{2}\|\mathbf{a}\| - \frac{1}{2}\|\mathbf{a}\|) \\ &= g(r). \end{aligned} \quad (131)$$

The lemma follows from (130) and (131).  $\square$

**Corollary/Definition 1** *There exists a constant  $\sigma_5 > 0$  such that for all  $\sigma \leq \sigma_5$  and all  $\widehat{\mathbf{s}} \in \mathbb{S}^{d-1}$ ,  $\text{RadialDomain}(\widehat{\mathbf{s}}, \sigma)$  is a closed interval. Thus, there is a function*

$$r^* : \mathbb{S}^{d-1} \times [0, \sigma_5] \rightarrow \mathbb{R}_{\geq 0} \quad \text{such that} \quad \text{RadialDomain}(\widehat{\mathbf{s}}, \sigma) =: [0, r^*(\widehat{\mathbf{s}}, \sigma)]. \quad (132)$$

*Proof* Take  $\sigma_5 := \min(c_7/c_6, \sigma_4) > 0$ , and let  $\sigma \leq \sigma_5$ . By  $\sigma \leq \sigma_4$ , Lemma 2 tells  $\text{RadialDomain}(\widehat{\mathbf{s}}, \sigma) \subseteq [0, c_6\sigma]$ . By  $\sigma \leq c_7/c_6$ , it holds  $[0, c_6\sigma] \subseteq [0, c_7]$ . By Lemma 3, for each  $\widehat{\mathbf{s}} \in \mathbb{S}^{d-1}$ ,  $r \mapsto G(\widehat{\mathbf{s}}, r)$  is strictly increasing over  $r \in [0, c_7]$ . The result follows.  $\square$

**Lemma 4** *There exists a constant  $\sigma_6 > 0$  such that the restriction of  $r^*$  to  $\mathbb{S}^{d-1} \times [0, \sigma_6]$  is a continuous function.*

*Proof* Take  $\sigma_6 = \sigma_5/2$ . We shall verify continuity of  $r^*$  by bare hands. For notational convenience, within this proof, we denote the second argument of  $r^*$  by  $\tau$  (subscripted and/or primed) rather than by  $\sigma$ . Fix  $(\widehat{\mathbf{s}}_1, \tau_1) \in \mathbb{S}^{d-1} \times [0, \sigma_6]$  and let  $\epsilon > 0$ .

Lemma 3 says  $r \mapsto G(\widehat{\mathbf{s}}_1, r)$  is continuous and strictly increasing around 0. By elementary facts, this has a well-defined continuous inverse function around  $G(0) = 0$ . The inverse function is  $\tau \mapsto r^*(\widehat{\mathbf{s}}_1, \tau)$  defined for  $\tau \in [0, \sigma_5]$  (Lemma 1). So, we can take  $\delta' \in (0, \sigma_6)$  such that for all  $\tau'_2 \in [0, \sigma_5]$ ,

$$|\tau'_2 - \tau_1| < \delta' \implies |r^*(\widehat{\mathbf{s}}_1, \tau'_2) - r^*(\widehat{\mathbf{s}}_1, \tau_1)| < \epsilon. \quad (133)$$

Since  $L_{\mathbf{p}}, Q_{\mathbf{p}}$  are continuous, there exist  $\delta'', \delta''' > 0$  such that for all  $\widehat{\mathbf{s}}_2 \in \mathbb{S}^{d-1}$ ,

$$\|\widehat{\mathbf{s}}_2 - \widehat{\mathbf{s}}_1\|_2 < \delta'' \implies \|L_{\mathbf{p}}(\widehat{\mathbf{s}}_2) - L_{\mathbf{p}}(\widehat{\mathbf{s}}_1)\| < \frac{1}{c_7} \frac{\delta'}{3}, \quad (134)$$

$$\|\widehat{\mathbf{s}}_2 - \widehat{\mathbf{s}}_1\|_2 < \delta''' \implies \left\| \frac{1}{2} Q_{\mathbf{p}}(\widehat{\mathbf{s}}_2) - \frac{1}{2} Q_{\mathbf{p}}(\widehat{\mathbf{s}}_1) \right\| < \frac{1}{c_7^2} \frac{\delta'}{3}. \quad (135)$$

Define  $\delta := \min\left(\frac{\delta'}{3}, \delta'', \delta'''\right) > 0$ . Let  $(\widehat{\mathbf{s}}_2, \tau_2) \in \mathbb{S}^{d-1} \times [0, \sigma_6]$  satisfy  $\|(\widehat{\mathbf{s}}_2, \tau_2) - (\widehat{\mathbf{s}}_1, \tau_1)\|_2 < \delta$ . We shall verify  $|r^*(\widehat{\mathbf{s}}_2, \tau_2) - r^*(\widehat{\mathbf{s}}_1, \tau_1)| < \epsilon$ .

Put  $r_1 := r^*(\widehat{\mathbf{s}}_1, \tau_1)$ ,  $r_2 := r^*(\widehat{\mathbf{s}}_2, \tau_2)$  and  $\tau'_2 := G(\widehat{\mathbf{s}}_1, r_2)$ . By (133), it suffices to check  $|\tau'_2 - \tau_1| < \delta'$ , as then  $\tau'_2 \in [0, \sigma_5]$  (because  $\tau'_2 \leq \tau_1 + \delta' \leq 2\sigma_6 = \sigma_5$ ) and also  $r^*(\widehat{\mathbf{s}}_1, \tau'_2) = r^*(\widehat{\mathbf{s}}_1, G(\widehat{\mathbf{s}}_1, r_2)) = r_2$ . So, (133) gives  $|r_2 - r_1| < \epsilon$ .

To see  $|\tau'_2 - \tau_1| < \delta$  indeed holds, we write

$$\begin{aligned} \tau'_2 &= \left\| r_2 L_{\mathbf{p}}(\widehat{\mathbf{s}}_1) + r_2^2 \frac{1}{2} Q_{\mathbf{p}}(\widehat{\mathbf{s}}_1) \right\| = \\ &= \left\| (r_2 L_{\mathbf{p}}(\widehat{\mathbf{s}}_2) + r_2^2 \frac{1}{2} Q_{\mathbf{p}}(\widehat{\mathbf{s}}_2)) + r_2 (L_{\mathbf{p}}(\widehat{\mathbf{s}}_1) - L_{\mathbf{p}}(\widehat{\mathbf{s}}_2)) + r_2^2 \left( \frac{1}{2} Q_{\mathbf{p}}(\widehat{\mathbf{s}}_2) - \frac{1}{2} Q_{\mathbf{p}}(\widehat{\mathbf{s}}_1) \right) \right\|. \end{aligned} \quad (136)$$

Using the triangle inequality, (134), (135) and  $r_2 \leq c_7$  (from the proof of Lemma 1),

$$|\tau'_2 - \tau_1| \leq |\tau_2 - \tau_1| + |\tau'_2 - \tau_2| < \frac{\delta'}{3} + c_7 \frac{1}{c_7} \frac{\delta'}{3} + c_7^2 \frac{1}{c_7^2} \frac{\delta'}{3} = \delta'. \quad (137)$$

This proves  $r^*$  is continuous on  $\mathbb{S}^{d-1} \times [0, \sigma_6]$ , when  $\sigma_6 = \sigma_5/2$ .  $\square$

**Lemma 5** *There exist constants  $c_8 \geq 0$  and  $\sigma_7 > 0$  such that for all  $\sigma \leq \sigma_7$  and all  $\widehat{\mathbf{s}} \in \mathbb{S}^{d-1}$ ,*

$$\frac{1}{\|L_{\mathbf{p}}(\widehat{\mathbf{s}})\|} \sigma - c_8 \sigma^2 \leq r^*(\widehat{\mathbf{s}}, \sigma) \leq \frac{1}{\|L_{\mathbf{p}}(\widehat{\mathbf{s}})\|} \sigma + c_8 \sigma^2. \quad (138)$$

*Proof* We will prove we may take

$$c_8 = \frac{\max_{\widehat{\mathbf{s}} \in \mathbb{S}^{d-1}} \|Q_{\mathbf{p}}(\widehat{\mathbf{s}})\|}{\min_{\widehat{\mathbf{s}} \in \mathbb{S}^{d-1}} \|L_{\mathbf{p}}(\widehat{\mathbf{s}})\|^3}. \quad (139)$$

Given  $\widehat{\mathbf{s}} \in \mathbb{S}^{d-1}$ . Let  $\mathbf{a} := L_{\mathbf{p}}(\widehat{\mathbf{s}})$ ,  $\mathbf{b} := \frac{1}{2}Q_{\mathbf{p}}(\widehat{\mathbf{s}})$ ,  $a := \|\mathbf{a}\|$  and  $b := \|\mathbf{b}\|$ . If  $\mathbf{b} = 0$ , then  $r^*(\widehat{\mathbf{s}}, \sigma) = (1/a)\sigma$  for all  $\sigma \geq 0$ , so (138) is obviously satisfied. Assume  $\mathbf{b} \neq 0$ . The triangle inequality gives

$$g_-(r) \leq g(r) \leq g_+(r) \quad \text{for all } r \in \mathbb{R}_{\geq 0}, \quad (140)$$

where  $g(r) := G(\widehat{\mathbf{s}}, r) = \|r\mathbf{a} + r^2\mathbf{b}\|$ ,  $g_-(r) := ar - br^2$  and  $g_+(r) := ar + br^2$ . Note  $g_+$  is strictly increasing over  $r \in [0, \infty)$ , while  $g_-$  is strictly increasing over  $r \in [0, \frac{a}{2b}]$  and  $g_-(\frac{a}{2b}) = \frac{a^2}{4b}$ . Let

$$\sigma'_6 := \min \left( \sigma_5, \frac{\min_{\widehat{\mathbf{s}} \in \mathbb{S}^{d-1}} \|L_{\mathbf{p}}(\widehat{\mathbf{s}})\|^2}{4 \max_{\widehat{\mathbf{s}} \in \mathbb{S}^{d-1}} \|Q_{\mathbf{p}}(\widehat{\mathbf{s}})\|} \right) > 0. \quad (141)$$

It follows from (140) and the intermediate value theorem that for all  $\sigma \in [0, \sigma'_7]$ ,

$$r_{+,+}^*(\sigma) \leq r^*(\sigma) \leq r_{-,-}^*(\sigma), \quad (142)$$

where  $r_{+,+}^*(\sigma)$  denotes the greater of the two roots in  $r$  to the quadratic equation  $g_+(r) = \sigma$  and where  $r_{-,-}^*(\sigma)$  denotes the lesser of the two roots in  $r$  to  $g_-(r) = \sigma$ . Explicitly, by the quadratic formula and Taylor series for the square root function,

$$\begin{aligned} r_{+,+}^*(\sigma) &:= \frac{-a + \sqrt{a^2 + 4b\sigma}}{2b} = \frac{1}{a}\sigma - \frac{b}{a^3}\sigma^2 + O(\sigma^3), \\ r_{-,-}^*(\sigma) &:= \frac{a - \sqrt{a^2 - 4b\sigma}}{2b} = \frac{1}{a}\sigma + \frac{b}{a^3}\sigma^2 + O(\sigma^3). \end{aligned} \quad (143)$$

On the other hand, from compactness of  $\mathbb{S}^{d-1}$ , one can check the implicit constants suppressed by the big  $O$  notation in (143) may all be taken independently of  $\widehat{\mathbf{s}}$ . At the same time,  $\frac{2b}{a^3} \leq c_8$  for each  $\widehat{\mathbf{s}} \in \mathbb{S}^{d-1}$ , by the definition (139). Taking  $\sigma_7 > 0$  to be sufficiently smaller than  $\sigma'_7$  yields the lemma.  $\square$

**Definition 4** Set  $\sigma_8 := \min(\sigma_6, \sigma_7) > 0$ . Define  $\eta^* : \mathbb{S}^{d-1} \times (0, \sigma_8] \rightarrow \mathbb{R}$  by

$$r^*(\widehat{\mathbf{s}}, \sigma) =: \frac{1}{\|L_{\mathbf{p}}(\widehat{\mathbf{s}})\|} \sigma + \frac{1}{2} \eta^*(\widehat{\mathbf{s}}, \sigma) \sigma^2. \quad (144)$$

By Lemma 4,  $\frac{1}{2}\eta^*$  is continuous. By Lemma 5, it is bounded uniformly in absolute value by  $2c_8$ .

### 3.8 Step 8: obtain $\text{tilt}_{\mathcal{M}, \mathcal{B}, \mathbf{p}}$ and apply dominated convergence

It remains to establish Equation (120): that is, to obtain the first-order term in the limiting differential operator. We do this using spherical coordinates (Subsection 3.6) and the results about the radial integration domain developed in Subsection 3.7. By swapping the order of limit and the integration (justified by dominated convergence), the tilt function emerges at last.

**Proposition 3** For each  $\widehat{\mathbf{s}} \in \mathbb{S}^{d-1}$ ,

$$\lim_{\sigma \rightarrow 0} \frac{1}{2} \eta^*(\widehat{\mathbf{s}}, \sigma) = \text{tilt}_{\mathcal{M}, \mathcal{B}, \mathbf{p}}(\widehat{\mathbf{s}}). \quad (145)$$

In particular, the limit on the LHS exists.

*Proof* By the bound (138) and compactness of  $[-c_8, c_8]$ , it suffices to show that every accumulation point of  $\frac{1}{2} \eta^*(\widehat{\mathbf{s}}, \sigma)$  as  $\sigma \rightarrow 0$  equals  $\text{tilt}_{\mathcal{M}, \mathcal{B}, \mathbf{p}}(\widehat{\mathbf{s}})$ . That is, assume  $(\tau_k)_{k=1}^\infty \subseteq (0, \sigma_8]$  is such that  $\tau_k \rightarrow 0$  and  $\frac{1}{2} \eta^*(\widehat{\mathbf{s}}, \tau_k) \rightarrow \eta \in [-c_8, c_8]$  as  $k \rightarrow \infty$ ; we will show  $\eta = \text{tilt}_{\mathcal{M}, \mathcal{B}, \mathbf{p}}(\widehat{\mathbf{s}})$ .

Substituting (144) into (132), and putting  $\mathbf{a} = L_{\mathbf{p}}(\widehat{\mathbf{s}})$ ,  $\mathbf{b} = \frac{1}{2} Q_{\mathbf{p}}(\widehat{\mathbf{s}})$ ,  $\eta_k = \eta(\widehat{\mathbf{s}}, \tau_k)$ , gives

$$\tau_k = \left\| \left( \frac{\tau_k}{\|\mathbf{a}\|} + \frac{1}{2} \eta_k \tau_k^2 \right) \mathbf{a} + \left( \frac{\tau_k}{\|\mathbf{a}\|} + \frac{1}{2} \eta_k \tau_k^2 \right)^2 \mathbf{b} \right\|. \quad (146)$$

Rearranging and dividing by  $\tau_k$ , this reads

$$1 = \left\| \frac{\mathbf{a}}{\|\mathbf{a}\|} + \left( \frac{1}{2} \eta_k \mathbf{a} + \frac{\mathbf{b}}{\|\mathbf{a}\|^2} \right) \tau_k + \frac{\eta_k \mathbf{b}}{\|\mathbf{a}\|} \tau_k^2 + \frac{\eta_k^2 \mathbf{b}}{4} \tau_k^3 \right\|. \quad (147)$$

By the definition of tangent cones, (147) witnesses that

$$\frac{\mathbf{b}}{\|\mathbf{a}\|^2} + \eta \mathbf{a} \in TC_{\mathbf{a}/\|\mathbf{a}\|}(\partial \mathcal{B}). \quad (148)$$

Indeed, in the definition (22), take  $\mathcal{Y} = \partial \mathcal{B} \subseteq \mathbb{R}^D$ ;  $\mathbf{y} = \mathbf{a}/\|\mathbf{a}\| \in \partial \mathcal{B}$ ;  $\mathbf{y}_k = \frac{\mathbf{a}}{\|\mathbf{a}\|} + \left( \frac{1}{2} \eta_k \mathbf{a} + \frac{\mathbf{b}}{\|\mathbf{a}\|^2} \right) \tau_k + \frac{\eta_k \mathbf{b}}{\|\mathbf{a}\|} \tau_k^2 + \frac{\eta_k^2 \mathbf{b}}{4} \tau_k^3 \in \partial \mathcal{B}$ ; the same  $\tau_k$ ; and  $\mathbf{d} = \frac{\mathbf{b}}{\|\mathbf{a}\|^2} + \eta \mathbf{a}$ . Then, (148) follows because  $(\mathbf{y}_k - \mathbf{y})/\tau_k = \left( \frac{1}{2} \eta_k \mathbf{a} + \frac{\mathbf{b}}{\|\mathbf{a}\|^2} \right) + \frac{\eta_k \mathbf{b}}{\|\mathbf{a}\|} \tau_k + \frac{\eta_k^2 \mathbf{b}}{4} \tau_k^2 \rightarrow \mathbf{d}$  as  $k \rightarrow \infty$ , using  $\frac{1}{2} \eta_k \rightarrow \eta$ ,  $\tau_k \rightarrow 0$ ,  $\eta_k = O(1)$  (Lemma 5) as  $k \rightarrow \infty$ . From Proposition/Definition 1 and the membership (148),  $\eta = \text{tilt}_{\mathcal{M}, \mathcal{B}, \mathbf{p}}(\widehat{\mathbf{s}})$ .  $\square$

*Finishing the proof of Theorem 1:* From the end of Subsection 3.5, it remains to establish (120). For  $\sigma \leq \min(\sigma_5, \sigma_6, \sigma_7, \sigma_8)$ , we have

$$\begin{aligned}
& \frac{1}{\sigma^{d+2}} \int_{\mathbf{s} \in \text{Approx}_2(\sigma)} \mathbf{s} d\mathbf{s} \\
&= \frac{1}{\sigma^{d+2}} \int_{\widehat{\mathbf{s}} \in \mathbb{S}^{d-1}} \widehat{\mathbf{s}} \int_{r \in \text{RadialDomain}(\widehat{\mathbf{s}}, \sigma)} r^d dr d\widehat{\mathbf{s}} \quad [(122)] \\
&= \frac{1}{\sigma^{d+2}} \int_{\widehat{\mathbf{s}} \in \mathbb{S}^{d-1}} \widehat{\mathbf{s}} \int_{r=0}^{r^*(\widehat{\mathbf{s}}, \sigma)} r^d dr d\widehat{\mathbf{s}} \quad [(132), \sigma \leq \sigma_5] \\
&= \frac{1}{\sigma^{d+2}} \int_{\widehat{\mathbf{s}} \in \mathbb{S}^{d-1}} \frac{\widehat{\mathbf{s}}}{d+1} \left( \frac{1}{\|L_{\mathbf{p}}(\widehat{\mathbf{s}})\|} \sigma + \frac{1}{2} \eta^*(\widehat{\mathbf{s}}, \sigma) \sigma^2 \right)^{d+1} d\widehat{\mathbf{s}} \quad [(144), \sigma \leq \sigma_8] \\
&= \frac{1}{(d+1)\sigma} \int_{\widehat{\mathbf{s}} \in \mathbb{S}^{d-1}} \frac{\widehat{\mathbf{s}}}{\|L_{\mathbf{p}}(\widehat{\mathbf{s}})\|^{d+1}} d\widehat{\mathbf{s}} \\
&+ \int_{\widehat{\mathbf{s}} \in \mathbb{S}^{d-1}} \widehat{\mathbf{s}} \left( \frac{\frac{1}{2} \eta^*(\widehat{\mathbf{s}}, \sigma)}{\|L_{\mathbf{p}}(\widehat{\mathbf{s}})\|^d} + O(\sigma) \right) d\widehat{\mathbf{s}} \quad [(138), \sigma \leq \sigma_7, \|L_{\mathbf{p}}(\widehat{\mathbf{s}})\|^{-1} = \omega(1)] \\
&= \int_{\widehat{\mathbf{s}} \in \mathbb{S}^{d-1}} \widehat{\mathbf{s}} \left( \frac{\frac{1}{2} \eta^*(\widehat{\mathbf{s}}, \sigma)}{\|L_{\mathbf{p}}(\widehat{\mathbf{s}})\|^d} + O(\sigma) \right) d\widehat{\mathbf{s}} \quad [\text{oddness}] \\
&\xrightarrow[\sigma \rightarrow 0]{\sigma \rightarrow 0} \lim_{\sigma \rightarrow 0} \int_{\widehat{\mathbf{s}} \in \mathbb{S}^{d-1}} \widehat{\mathbf{s}} \frac{\frac{1}{2} \eta^*(\widehat{\mathbf{s}}, \sigma)}{\|L_{\mathbf{p}}(\widehat{\mathbf{s}})\|^d} d\widehat{\mathbf{s}} \\
&= \int_{\widehat{\mathbf{s}} \in \mathbb{S}^{d-1}} \widehat{\mathbf{s}} \|L_{\mathbf{p}}(\widehat{\mathbf{s}})\|^{-d} \lim_{\sigma \rightarrow 0} \frac{1}{2} \eta^*(\widehat{\mathbf{s}}, \sigma) d\widehat{\mathbf{s}} \quad [\text{dominated convergence}] \\
&= \int_{\widehat{\mathbf{s}} \in \mathbb{S}^{d-1}} \widehat{\mathbf{s}} \|L_{\mathbf{p}}(\widehat{\mathbf{s}})\|^{-d} \text{tilt}_{\mathcal{M}, \mathcal{B}, \mathbf{p}}(\widehat{\mathbf{s}}) d\widehat{\mathbf{s}}. \quad [(145)]
\end{aligned} \tag{149}$$

The use of dominated convergence is justified because  $\widehat{\mathbf{s}} \mapsto \frac{1}{2} \eta^*(\widehat{\mathbf{s}}, \sigma)$  is continuous in  $\widehat{\mathbf{s}}$  for each  $\sigma \leq \sigma_6$  (Lemma 4), it is uniformly bounded in absolute value by  $c_8$  for each  $\sigma \leq \sigma_7$  (Lemma 5), and  $\lim_{\sigma \rightarrow 0} \frac{1}{2} \eta^*(\widehat{\mathbf{s}}, \sigma)$  exists and equals  $\text{tilt}_{\mathcal{M}, \mathcal{B}, \mathbf{p}}$  (Proposition 3). This completes the proof of Theorem 1.  $\square$

#### 4 Numerical simulation: learning shape spaces

In this section, we present an application of manifold learning based on a non-Euclidean norm for learning volumetric shape spaces. The motivation comes from the field of cryo-electron microscopy [52]; more specifically, from the analysis of flexible proteins and other large molecules with moving parts [17, 53,

30]. Several works have applied diffusion maps to this problem [15, 45, 14]. In a recent paper, we proposed to use a variant of diffusion maps with a wavelet-based approximate Earthmover’s distance (EMD) for the dimensionality reduction of molecular volume spaces [62]. EMD measures the minimal amount of mass transfer needed to convert one probability distribution into another and therefore provides a distance metric that is meaningful even between spatial conformations that are far from each other. In [62], we demonstrated that, compared to standard (Euclidean) diffusion maps, the EMD-based diffusion maps can require far less samples to recover the intrinsic conformational manifold. This section extends our previous work with two important differences:

1. In [62], we used Coifman and Lafon’s density-normalizing reweighting of the affinity matrix [11]. In contrast, here we use the plain (unweighted) graph Laplacian, to match with our theoretical results in the present paper.
2. Smoothness in the volumetric signals induces sparsity in the resulting wavelet coefficients. Here, we demonstrate in Subsection 4.3 how to exploit this phenomenon to significantly reduce the running time and memory requirements of the new procedure. This results in a method that is much faster than Euclidean diffusion maps.

We briefly mention some related works that combine the Earthmover’s distance with graph Laplacian methods: In [43, 42] tree-based metrics [13] were used as a basis for diffusion maps. These metrics can be interpreted as a hierarchical Earthmover’s distance. However, since the trees are data dependent, our Theorem 1 does not apply. Another work which combines diffusion maps and the Earthmover’s distance first computes Euclidean diffusion maps and then applies the Earthmover’s distance to the resulting point clouds [38].

#### 4.1 Method

Given a set of volumetric arrays  $\mathbf{x}_1, \dots, \mathbf{x}_n \in \mathcal{M} \subseteq \mathbb{R}^{L^3}$ , we compute an approximate Earthmover’s distance between all pairs of points [50]. This involves first computing the discrete wavelet transform of all the inputs and then using a weighted  $\ell_1$ -norm on the pairwise differences of wavelet coefficients,

$$\|\mathbf{x}_i - \mathbf{x}_j\|_{\text{WEMD}} := \sum_{\lambda} 2^{-5s/2} |\mathcal{W}\mathbf{x}_i(\lambda) - \mathcal{W}\mathbf{x}_j(\lambda)|. \quad (150)$$

Here,  $\mathcal{W}\mathbf{x}$  denotes the 3D wavelet transform of  $\mathbf{x}$ . The index  $\lambda$  contains the wavelet shifts  $(m_1, m_2, m_3) \in \mathbb{Z}^3$  and scale parameter  $s \in \mathbb{Z}_{\geq 0}$ . We then compute pairwise Gaussian affinities,

$$W_{ij} = \exp(-\|\mathbf{x}_i - \mathbf{x}_j\|_{\text{WEMD}}^2 / \sigma^2), \quad (151)$$

proceed to construct a graph Laplacian, and perform the eigenvector-based embedding as described in Subsection 1.2. See [50] for more details on the wavelet-based approximation to the Earthmover’s distance.

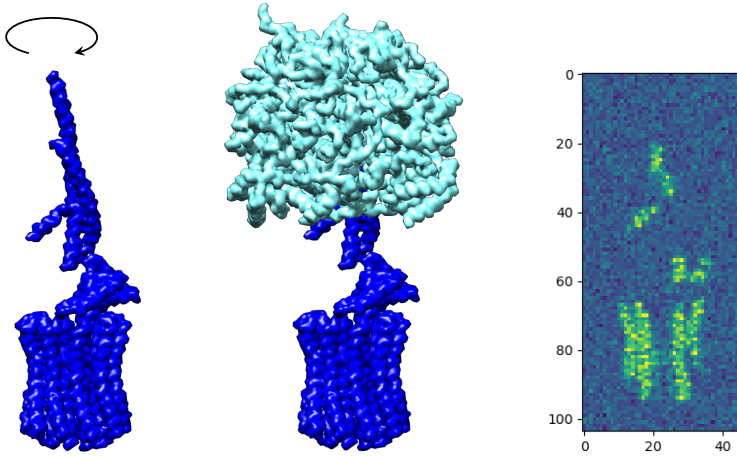


**Fig. 3** *ATP synthase*. (left)  $F_0$  and axle subunits. These jointly rotate in the presence of hydrogen ions, together forming a molecular electric motor; (middle) the  $F_1$  subunit (in cyan) envelops the axle. As the axle rotates, the  $F_1$  subunit assembles ATP; (right) representative 2D slice of the rotated  $F_0$  and axle subunits, with additive noise shown.

#### 4.2 Data set generation and simulation results

To test the proposed EMD-based dimensionality reduction procedure, we generated a synthetic volumetric data set which mimics the motion space of ATP synthase [61], see Figure 3. This enzyme is a stepper motor with a central asymmetric axle that rotates in  $120^\circ$  steps relative to the  $F_1$  subunit, with short transient motions in-between the three dominant states. Here, the intrinsic geometry is a circle, with a sampling density concentrated around three equi-spaced angles. See [62] for more details on this data set. Figure 4 compares the Euclidean distance to the wavelet-based approximate Earthmover’s distance (WEMD) for a range of angular differences using the noiseless data set. We then performed a two-dimensional diffusion map embedding, shown in Figure 5, using both the Euclidean ( $\ell_2$ ) distance and the norm WEMD 150. Some technical notes regarding Figure 5:

- The 3D discrete wavelet transform was computed using PyWavelets [33] with the `sym3` wavelet, up to scale level  $s = 6$  to minimize the truncation in Equation (150). The number of resulting wavelet coefficients was 40% larger than the number of voxels.
- The embeddings shown here use the unweighted graph Laplacian with a Gaussian kernel, since this exactly matches the theory presented in this paper. For similar embedding results that use Coifman and Lafon’s density normalizing diffusion maps [11], see Figure 5 in our previous paper [62].
- We chose  $\sigma = 30$  as the Gaussian kernel width in Equation (151) for the WEMD embeddings, however the WEMD results are not very sensitive to the particular choice of  $\sigma$ . In contrast, the Euclidean embeddings required fine-tuning of  $\sigma$  to obtain the best results for each sample size.



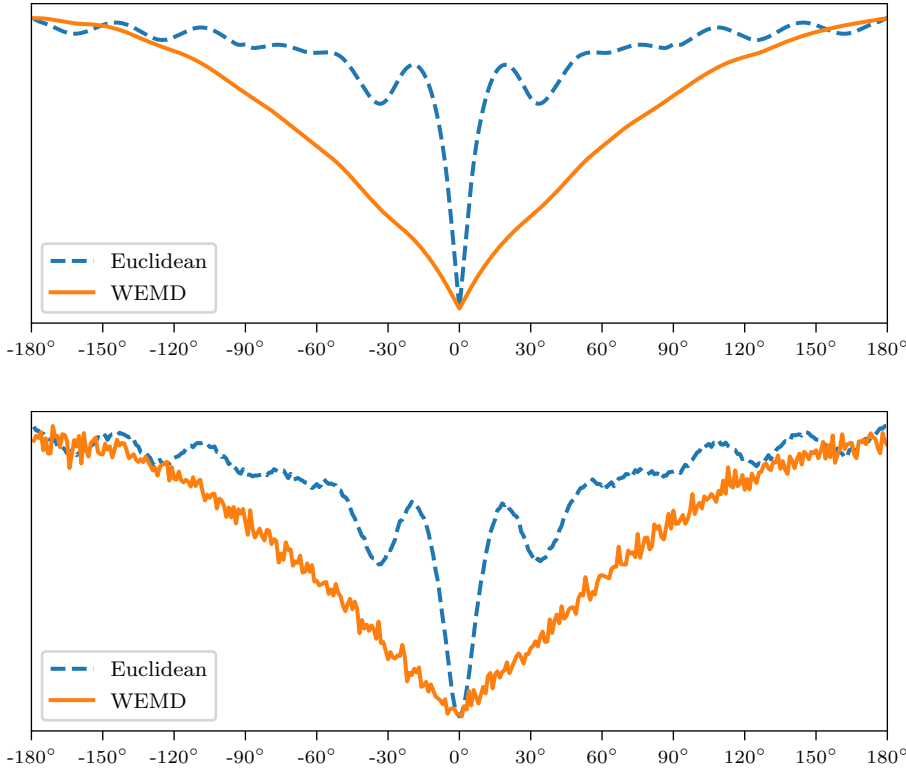


**Fig. 4** *Euclidean distance vs. wavelet-based approximate Earthmover’s distance (WEMD)* as functions of the angle between rotations of the ATP synthase rotor (recall the left panel of Figure 3). Here, the top graph displays results for rotated volumes without noise, while the bottom graph is for the noisy data set. The Euclidean distances were scaled to be comparable to the WEMD. Observe WEMD is monotonic in the magnitude of the angular difference for the entire range, whereas the  $\ell_2$  distance has this desirable behavior only up to about  $\pm 19^\circ$ .

The running time of the WEMD-based diffusion maps is similar to that of the standard Euclidean diffusion maps. This follows from the fact that both algorithms need to compute  $\binom{n}{2}$  pairwise  $\ell_p$  distances ( $p \in \{1, 2\}$ ) for vectors of similar length. The cost of the discrete wavelet transform is negligible, since it is linear with respect to the input size. For our sample sizes, the time to form the Gaussian affinity matrix and compute its eigenvectors is negligible. Table 1 lists single-core running times on an Intel Core i7-8569U CPU.

### 4.3 Exploiting wavelet sparsity

Recall that to compute the approximate Earthmover’s distance between all pairs of volumes, we first compute a weighted discrete wavelet transform of each volume in our data set. For smooth signals this results in sparse vectors of wavelet coefficients [40]. We may use this fact to our advantage by thresholding

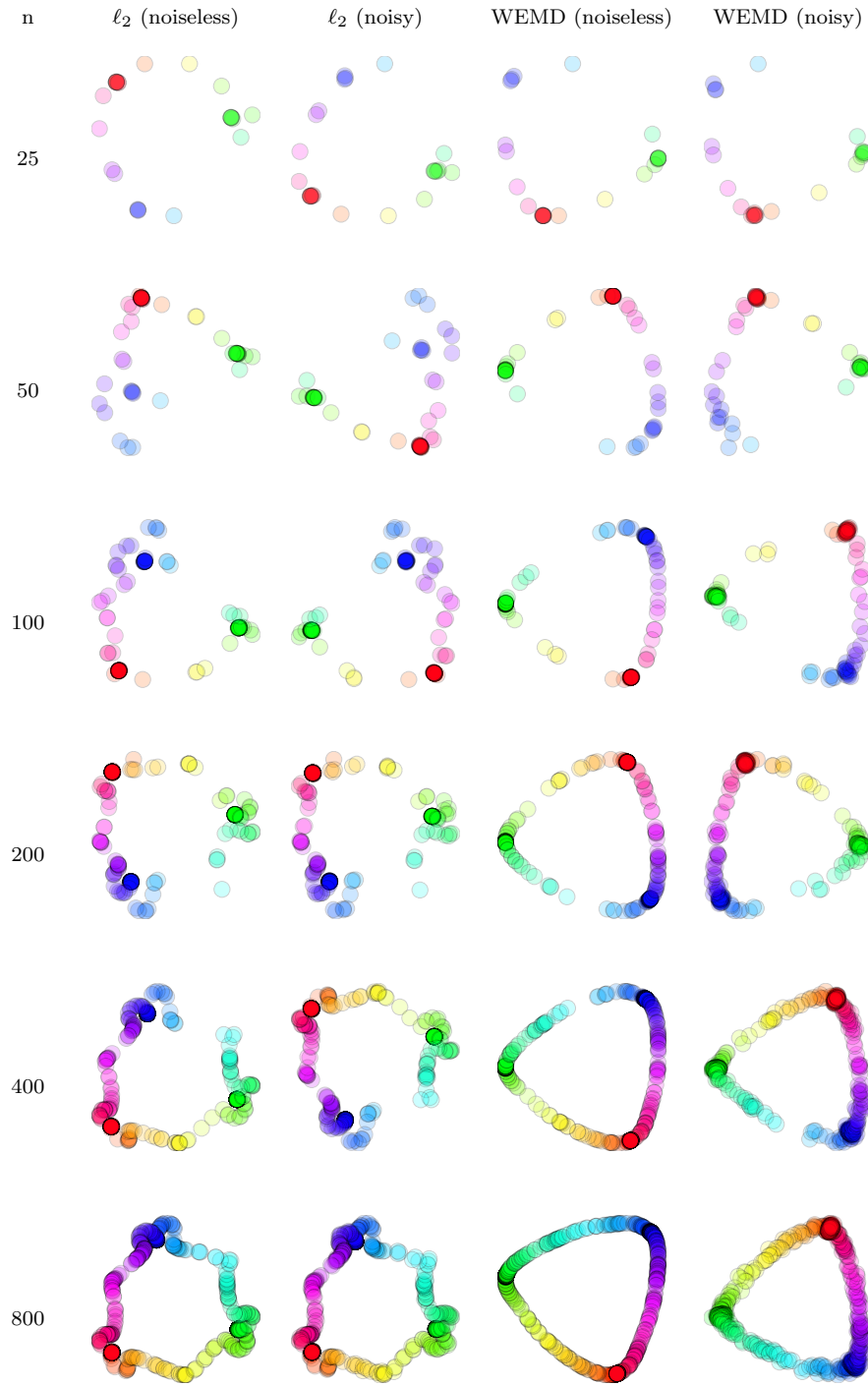


**Fig. 5** *Laplacian-based embeddings in  $\mathbb{R}^2$ .* Euclidean vs. wavelet-EMD-based diffusion mappings on the clean and noisy ATP synthase data sets, for sample sizes of  $n = 25, 50, 100, 200, 400, 800$ . The points are translucent to visually indicate density. Notice the high density around three angles  $120^\circ$  apart, in agreement with the data generation.

**Table 1** *Running times [sec]* for computing the discrete wavelet transform (DWT), all pairwise wavelet-based Earthmover approximations (WEMD) not including the DWT, and all pairwise Euclidean ( $\ell_2$ ) distances.

$n$	DWT	WEMD	$\ell_2$
25	0.3	0.13	0.09
50	0.61	0.49	0.38
100	1.2	1.93	1.5
200	2.4	7.6	5.5
400	4.9	31	22
800	11	126	86

the vectors of weighted wavelet coefficients and storing them in a sparse matrix. The computational benefit of this stems from the fact that computing the  $\ell_1$  distance between two sparse vectors has a runtime that is linear in the number of their non-zero elements. Since the computation of all pairwise  $\ell_1$  differences is the slowest part of our procedure, this approach can reduce the running time significantly.

We tested this idea on the ATP synthase data presented in the previous section. First, we subtracted the mean volume from all volumes in the data set. This does not change the pairwise WEMD distances but makes the resulting vectors more sparse. Let us denote by  $h_t$  the hard-thresholding function,

$$h_t(x) := \begin{cases} 0, & \text{for } |x| \leq t \\ x, & \text{for } |x| > t. \end{cases} \quad (152)$$

We find a threshold  $t$  such that the  $\ell_1$  norm of the weighted wavelet coefficients of the entire data set are 90% of the  $\ell_1$  norm of the data set prior to thresholding. This threshold was computed on the smallest simulation of size  $n = 25$  and applied to the rest of the runs. Figure 6 shows the results of WEMD embedding following this sparsification step. Table 2 shows the running times for the sparsified WEMD. Note that the running times are different for the noiseless and noisy data sets, since the noisy data is less sparse. In both cases, there are significant gains to the running times with no discernible change to the embedding results without sparsification (shown in Figure 5).

**Table 2** *Running times [sec]* for computing all pairs of sparsified wavelet-based Earthmover's distances (sparse-WEMD), as compared to the dense computation.

$n$	Sparse runtime (noiseless data)	Sparse runtime (noisy data)	Dense runtime
25	0.01	0.037	0.13
50	0.013	0.1	0.49
100	0.026	0.39	1.93
200	0.046	1.5	7.6
400	0.16	6.2	31
800	0.6	25	126

## 5 Conclusion

In this paper, we placed Laplacian-based manifold learning methods that use non-Euclidean norms on a firmer footing. For the first time, we proved the pointwise convergence of discrete graph Laplacians using general norms to a certain elliptic second-order continuous differential operator. The argument threw light on a novel second-order interaction between the manifold  $\mathcal{M}$  and the unit ball  $\mathcal{B}$ , encoded by the function  $\text{tilt}_{\mathcal{M},\mathcal{B},\mathbf{p}}$ . Some features of the Laplace-Beltrami operator do not survive in the general case: the limiting operator changes with the embedding of  $\mathcal{M}$  and it carries a first-order term that can exhibit discontinuities at certain points of  $\mathcal{M}$ . Theorem 1 reveals the exact tension between  $\mathcal{M}$  and  $\mathcal{B}$ .

In addition, this work demonstrated practical advantages for using non-Euclidean norms in manifold learning. We considered the task of learning molecular shape spaces, where data points are conformations (3D arrays), and we wish to capture the shape variation. A numerical simulation found that using diffusion maps with the wavelet Earthmover’s distance (a weighted  $\ell_1$  norm in wavelet coefficients) exhibits superior sample complexity compared to  $\ell_2$ . Exploiting wavelet sparsity, the non-Euclidean norm showed reduced computational cost. Further, it was observed to be more robust to noise than  $\ell_2$ .

Our investigation suggests a number of points worthy of further study. First and foremost, due to space limitations, we have deferred spectral analysis of  $\mathcal{L}_{\mathcal{M},\|\cdot\|}$  to future consideration, as well as a proof of stronger (spectral) convergence in Theorem 1. Neither have we determined convergence rates, although Figure 5 suggests that these should depend on the choice of  $\|\cdot\|$ . Further, it would be useful to have results for the case of normalized graph Laplacians. Also, we suspect that there are interesting questions around *high dimensionality*:  $\mathcal{L}_{\mathcal{M},\|\cdot\|}$  is governed by  $d$ - and 2-dimensional linear sections of the convex body  $\mathcal{B} \subseteq \mathbb{R}^D$ . When  $D \gg d$ , we wonder: do these slices look increasingly Euclidean, i.e., does  $\mathcal{L}_{\mathcal{M},\|\cdot\|}$  concentrate (in some suitable sense)?

Regarding applications, we hope our paper emboldens more practitioners to consider using non-Euclidean norms in manifold learning. As mentioned, this tack has been tried already (e.g., [43, 42]), however the theoretical support for doing so was not available. While our current theory does assume a fixed data-independent norm, we hope it increases general confidence that “non-Euclidean norms are probably okay”. This begs an important design question:

*For a given type of data set and analysis task, how should one select the best norm to use inside manifold learning?*

**Acknowledgements** The authors thank Charles Fefferman, William Leeb and Eitan Levin for enlightening discussions. This research was supported in parts by AFOSR FA9550-17-1-0291, ARO W911NF-17-1-0512, NSF BIGDATA IIS-1837992, the Simons Investigator Award, the Moore Foundation Data-Driven Discovery Investigator Award, the Simons Collaboration on Algorithms and Geometry, as well as start-up grants from the College of Natural Sciences and Oden Institute at the University of Texas at Austin.

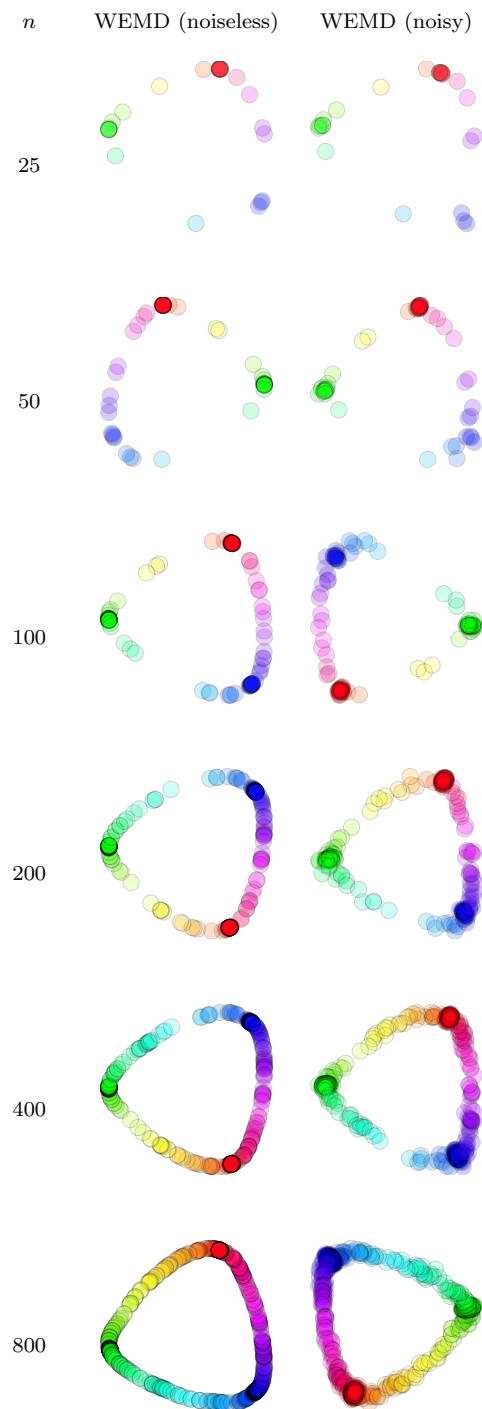


**Fig. 6** *Sparsified results.* Wavelet-EMD-based diffusion mappings of the clean and noisy ATP synthase data sets, after applying hard-thresholding to obtain sparse coefficient vectors.

## Appendices

### A Proof of Lemma 1

**Step 1: LHS  $\subseteq$  RHS.** By definition of  $\partial$  and of tangent cones (23), the LHS of (24) is

$$\partial(TC_{\mathbf{y}}(\mathcal{B})) = \overline{\mathbb{R}_{>0}(\mathcal{B} - \mathbf{y})} \setminus (\mathbb{R}_{>0}(\mathcal{B} - \mathbf{y}))^\circ. \quad (153)$$

Let  $\mathbf{d} \in \partial(TC_{\mathbf{y}}(\mathcal{B}))$ . By (153),  $\mathbf{d} = \lim_{k \rightarrow \infty} \beta_k(\tilde{\mathbf{y}}_k - \mathbf{y})$  for some  $\beta_k \in \mathbb{R}_{>0}$  and  $\tilde{\mathbf{y}}_k \in \mathcal{B}$ . Without loss of generality,  $\tilde{\mathbf{y}}_k \in \partial\mathcal{B}$  for each  $k$ ; indeed, whenever  $\tilde{\mathbf{y}}_k \neq \mathbf{y}$ , we may replace  $\tilde{\mathbf{y}}_k \leftarrow (\tilde{\mathbf{y}}_k - \mathbf{y}) / \|\tilde{\mathbf{y}}_k - \mathbf{y}\|$  and  $\beta_k \leftarrow \beta_k / \|\tilde{\mathbf{y}}_k - \mathbf{y}\|$ . Further, by compactness of  $\partial\mathcal{B}$ , we may assume  $\lim_{k \rightarrow \infty} \tilde{\mathbf{y}}_k = \tilde{\mathbf{y}}$  for some  $\tilde{\mathbf{y}} \in \partial\mathcal{B}$ , by passing to a subsequence if necessary. We break into cases.

– *Case A:  $\tilde{\mathbf{y}} = \mathbf{y}$ .*

Either  $\mathbf{d} = 0 \in T_{\mathbf{y}}(\partial\mathcal{B})$ , or  $\tau_k := 1/\beta_k \rightarrow \infty$  as  $k \rightarrow \infty$ . If the latter, the sequences  $(\tilde{\mathbf{y}}_k)_{k=1}^\infty \subseteq \partial\mathcal{B}$  and  $(\tau_k)_{k=1}^\infty \subseteq \mathbb{R}_{>0}$  witness  $\mathbf{d} \in TC_{\mathbf{y}}(\partial\mathcal{B})$ .

– *Case B:  $\tilde{\mathbf{y}} \neq \mathbf{y}$ .*

Here,  $\lim_{k \rightarrow \infty} \beta_k =: \beta \in \mathbb{R}_{\geq 0}$  exists, and  $\mathbf{d} = \beta(\tilde{\mathbf{y}} - \mathbf{y})$ . If  $\beta = 0$ , then  $\mathbf{d} = 0 \in T_{\mathbf{y}}(\partial\mathcal{B})$ . Suppose  $\beta \neq 0$ . Let the line segment joining  $\tilde{\mathbf{y}}$  and  $\mathbf{y}$  be

$$\text{conv}\{\tilde{\mathbf{y}}, \mathbf{y}\} := \{\alpha\tilde{\mathbf{y}} + (1 - \alpha)\mathbf{y} \in \mathbb{R}^D : \alpha \in [0, 1]\}. \quad (154)$$

So,  $\text{conv}\{\tilde{\mathbf{y}}, \mathbf{y}\} \subseteq \mathcal{B}$ . We claim  $\text{conv}\{\tilde{\mathbf{y}}, \mathbf{y}\} \subseteq \partial\mathcal{B}$ . Assume not. That is,

$$\exists \alpha \in (0, 1) \text{ such that } \mathbf{z} := \alpha\tilde{\mathbf{y}} + (1 - \alpha)\mathbf{y} \in \mathcal{B}^\circ. \quad (155)$$

But then,

$$\mathbf{d} = \beta(\tilde{\mathbf{y}} - \mathbf{y}) = (\beta/\alpha)(\mathbf{z} - \mathbf{y}) \in \mathbb{R}_{>0}(\mathcal{B}^\circ - \mathbf{y}) \subseteq (\mathbb{R}_{>0}(\mathcal{B} - \mathbf{y}))^\circ. \quad (156)$$

This contradicts  $\mathbf{d} \in \partial(TC_{\mathbf{y}}(\mathcal{B}))$  (see (153)). So, indeed  $\text{conv}\{\tilde{\mathbf{y}}, \mathbf{y}\} \subseteq \partial\mathcal{B}$ . Now, define

$$\hat{\mathbf{y}}_k := \frac{1}{k}\tilde{\mathbf{y}} + (1 - \frac{1}{k})\mathbf{y} \in \partial\mathcal{B} \quad \text{and} \quad \tau_k := \frac{1}{k} \in \mathbb{R}_{>0}. \quad (157)$$

Then,  $\frac{\hat{\mathbf{y}}_k - \mathbf{y}}{\tau_k} = \mathbf{d}$  for each  $k$ , and  $(\hat{\mathbf{y}}_k)_{k=1}^\infty$  and  $(\tau_k)_{k=1}^\infty$  witness  $\mathbf{d} \in TC_{\mathbf{y}}(\partial\mathcal{B})$ .

In all cases, we have verified  $\mathbf{d} \in TC_{\mathbf{y}}(\partial\mathcal{B})$ . This gives LHS  $\subseteq$  RHS in (24).

**Step 2: LHS  $\supseteq$  RHS.** Let  $\mathbf{d} \in TC_{\mathbf{y}}(\partial\mathcal{B})$ . By the definition of tangent cones (22),  $\mathbf{d} = \lim_{k \rightarrow \infty} \tau_k^{-1}(\tilde{\mathbf{y}}_k - \mathbf{y})$  for some  $\tau_k \in \mathbb{R}_{>0}$  and  $\tilde{\mathbf{y}}_k \in \partial\mathcal{B}$  with  $\tau_k \rightarrow 0$  and  $\tilde{\mathbf{y}}_k \rightarrow \mathbf{y}$  as  $k \rightarrow \infty$ . By (153), we need to show  $\mathbf{d} \notin (\mathbb{R}_{>0}(\mathcal{B} - \mathbf{y}))^\circ$ .

First, we will prove  $\text{conv}\{\mathbf{d} + \mathbf{y}, \mathbf{y}\} \cap \mathcal{B}^\circ = \emptyset$ . Assume not, i.e.,

$$\exists \alpha \in (0, 1) \text{ such that } \mathbf{z} := \alpha(\mathbf{d} + \mathbf{y}) + (1 - \alpha)\mathbf{y} = \alpha\mathbf{d} + \mathbf{y} \in \mathcal{B}^\circ. \quad (158)$$

Let  $\hat{\tau}_k = \tau_k/\alpha \in \mathbb{R}_{>0}$ , so that

$$\alpha\mathbf{d} = \lim_{k \rightarrow \infty} \hat{\tau}_k^{-1}(\tilde{\mathbf{y}}_k - \mathbf{y}). \quad (159)$$

Since  $\mathcal{B}^\circ$  is open, there exists  $\delta > 0$  with

$$\mathcal{N} := \{\mathbf{w} \in \mathbb{R}^D : \|\mathbf{w} - \mathbf{z}\|_2 \leq \delta\} \subseteq \mathcal{B}^\circ. \quad (160)$$

By (159), there exists  $K$  such that for all  $k \geq K$ ,

$$\hat{\tau}_k^{-1}(\tilde{\mathbf{y}}_k - \mathbf{y}) + \mathbf{y} \in \mathcal{N}. \quad (161)$$

On the other hand, it is easy to see for each  $\mathbf{w} \in \mathcal{B}^\circ$ ,

$$(\mathbf{y} + \mathbb{R}_{\geq 0}(\mathbf{w} - \mathbf{y})) \cap \mathcal{B} = \text{conv}\{\mathbf{y}, \mathbf{w}'\} \quad (162)$$

for some  $\mathbf{w}' \in \partial\mathcal{B}$ , using convexity and compactness of  $\mathcal{B}$ . In addition,

$$(\mathbf{y} + \mathbb{R}_{\geq 0}(\mathbf{w} - \mathbf{y})) \cap \partial\mathcal{B} = \{\mathbf{y}, \mathbf{w}'\}, \quad (163)$$

using  $\mathbf{w} \in \text{conv}\{\mathbf{y}, \mathbf{w}'\}$ ,  $\|\mathbf{w}\| < 1$ , and the triangle inequality for  $\|\cdot\|$ . Clearly,

$$\|\mathbf{w}' - \mathbf{y}\|_2 > \|\mathbf{w} - \mathbf{y}\|_2. \quad (164)$$

Now, let  $\epsilon := \min_{\mathbf{w} \in \mathcal{N}} \|\mathbf{w} - \mathbf{y}\|_2$ . Note  $\epsilon > 0$ . For each  $k \leq K$ , we apply (162), (163) to  $\mathbf{w} = \hat{\tau}_k^{-1}(\tilde{\mathbf{y}}_k - \mathbf{y}) + \mathbf{y} \in \mathcal{N}$ . Then,  $\mathbf{w}' = \tilde{\mathbf{y}}_k$ . By (164),

$$\|\tilde{\mathbf{y}}_k - \mathbf{y}\|_2 > \|\mathbf{w} - \mathbf{y}\|_2 \geq \epsilon \quad \text{for all } k \geq K. \quad (165)$$

But (165) contradicts  $\tilde{\mathbf{y}}_k \rightarrow \mathbf{y}$  as  $k \rightarrow \infty$ . Therefore,  $\text{conv}\{\mathbf{d} + \mathbf{y}, \mathbf{y}\} \cap \mathcal{B}^\circ = \emptyset$ .

Translating by  $-\mathbf{y}$ ,  $\text{conv}\{\mathbf{d}, 0\} \cap (\mathcal{B} - \mathbf{y})^\circ = \emptyset$ . By this and convexity, it follows there exists a properly separating hyperplane:

$$\begin{aligned} \exists \mathbf{v} \in \mathbb{R}^D \setminus \{0\}, \exists \gamma \in \mathbb{R} \text{ such that } \forall \mathbf{u}_1 \in \text{conv}\{\mathbf{d}, 0\}, \forall \mathbf{u}_2 \in \mathcal{B} - \mathbf{y} \\ \langle \mathbf{v}, \mathbf{u}_1 \rangle \geq \gamma, \langle \mathbf{v}, \mathbf{u}_2 \rangle \leq \gamma \text{ and } \exists \tilde{\mathbf{u}}_2 \in \mathcal{B} - \mathbf{y} \text{ such that } \langle \mathbf{v}, \tilde{\mathbf{u}}_2 \rangle < \gamma. \end{aligned} \quad (166)$$

In particular,

$$\mathbb{R}_{>0}(\mathcal{B} - \mathbf{y}) \subseteq \{\mathbf{u} \in \mathbb{R}^D : \langle \mathbf{v}, \mathbf{u} \rangle \leq \gamma\}. \quad (167)$$

Also, for any open neighborhood  $\mathcal{D} \subseteq \mathbb{R}^D$  with  $\mathbf{d} \in \mathcal{D}$ ,

$$\exists \tilde{\mathbf{d}} \in \mathcal{D} \text{ such that } \langle \mathbf{v}, \tilde{\mathbf{d}} \rangle > \langle \mathbf{v}, \mathbf{d} \rangle \geq \gamma. \quad (168)$$

We conclude  $\mathbf{d} \notin (\mathbb{R}_{>0}(\mathcal{B} - \mathbf{y}))^\circ$ , as desired. This gives  $\mathbf{d} \in \partial(TC_{\mathbf{y}}(\mathcal{B}))$ , and  $\text{LHS} \supseteq \text{RHS}$  in (24), completing the proof of the lemma.  $\square$

## B Tail bounds and absolute moments of the Gaussian

We recall some basic properties of the Gaussian. As in Subsection 3.2,  $\kappa_\sigma(s) := \frac{2s}{\sigma^2} e^{-s^2/\sigma^2}$ .

- For each even  $k \geq 0$  and  $\delta \geq 0$ , by substitution and then integration by parts  $k/2$  times,

$$\begin{aligned} \int_{s=\delta}^{\infty} s^k \kappa_\sigma(s) ds \\ = \sigma^k e^{-\delta^2/\sigma^2} \left( \left( \frac{\delta^2}{\sigma^2} \right)^{\frac{k}{2}} + \frac{k}{2} \left( \frac{\delta^2}{\sigma^2} \right)^{\frac{k}{2}-1} + \frac{k}{2} \left( \frac{k}{2} - 1 \right) \left( \frac{\delta^2}{\sigma^2} \right)^{\frac{k}{2}-2} + \dots + \left( \frac{k}{2} \right)! \right) \\ = e^{-\delta^2/\sigma^2} \text{poly}(\sigma, \delta). \end{aligned} \quad (169)$$

- For each odd  $k \geq 0$  and  $\delta > 0$ , using  $s/\delta \geq 1$  for  $s \in [\delta, \infty]$  and (169),

$$\int_{s=\delta}^{\infty} s^k \kappa_\sigma(s) ds \leq (1/\delta) \int_{s=\delta}^{\infty} s^{k+1} \kappa_\sigma(s) ds = e^{-\delta^2/\sigma^2} (1/\delta) \text{poly}(\sigma, \delta). \quad (170)$$

- For each  $k \geq 0$ , from [60, Equation 18],

$$\int_{s=0}^{\infty} s^k \kappa_\sigma(s) ds = \sigma^k \Gamma\left(\frac{k+2}{2}\right). \quad (171)$$

## C Numerical estimation of one-dimensional eigenfunctions

The eigenfunctions of the limiting operator are of key interest for manifold learning methods in general. For the case of the circle example (Subsection 2.6), these are the functions  $\varphi : [0, 2\pi] \rightarrow \mathbb{R}$  that solve the following generalized Helmholtz boundary value problem:

$$\mathcal{L}\varphi + \lambda\varphi = 0, \quad (172)$$

where the Laplacian  $\mathcal{L}$  is the limiting differential operator in Equation (63), subject to the periodic boundary conditions,

$$\varphi(\theta + 2\pi) = \varphi(\theta), \quad (173)$$

$$\varphi'(\theta + 2\pi) = \varphi'(\theta). \quad (174)$$

Figure 7 shows numerically computed solutions of Equation (172) for different choices of  $w_1, w_2$ . Notice the eigenfunctions are oscillatory, as dictated by Sturm-Liouville theory [1].

We describe the numerical computation of these limiting eigenfunctions. We used a standard finite-differences scheme where the first derivative was replaced by a symmetrized difference

$$\frac{df}{d\theta} \rightarrow \frac{f(\theta + \Delta\theta) - f(\theta - \Delta\theta)}{2\Delta\theta}, \quad (175)$$

and the second derivative by

$$\frac{d^2f}{d\theta^2} \rightarrow \frac{f(\theta + \Delta\theta) - 2f(\theta) + f(\theta - \Delta\theta)}{(\Delta\theta)^2}. \quad (176)$$

In this equation,  $f$  is taken to be a cyclic function defined over the discrete range

$$\left\{ 0, \frac{2\pi}{n}, \dots, \frac{2\pi(n-1)}{n} \right\}. \quad (177)$$

To compute the solutions we formed a sparse  $n \times n$  matrix  $L$  that corresponds to the finite-difference operator formed by substituting (175) and (176) into the first and second derivative terms in Equation (172). The eigenvalues and eigenvectors of  $L$  were found using the function `scipy.sparse.linalg.eigs()` from the SciPy package [57]. It is a wrapper of the ARPACK library for large-scale eigenvalue problems [36]. Recall that in our problem, all eigenvalues are non-positive. To obtain the smallest (in magnitude) eigenvalues and their corresponding eigenvectors, we used the `eigs()` function in shift-invert mode with  $\sigma = 1$ . The particular choice of  $\sigma$  did not seem to matter much when  $\sigma > 0$ , however choosing  $\sigma = 0$  resulted in instabilities and convergence errors. This is due to the fact that shift-invert mode attempts to find solutions to  $(L - \sigma I)^{-1}\mathbf{x} = \lambda\mathbf{x}$ , and since zero is an eigenvalue of  $L$ , the choice  $\sigma = 0$  results in the inversion of an ill-conditioned matrix. The use of sparse matrices allows one to take large values of  $n$ , since applying the finite-differences operator defined above costs only  $O(n)$ .

## References

1. Al-Gwaiz, M.: Sturm-Liouville theory and its applications. Springer London, London (2008). doi:[10.1007/978-1-84628-972-9](https://doi.org/10.1007/978-1-84628-972-9)
2. Arias-Castro, E., Le Gouic, T.: Unconstrained and curvature-constrained shortest-path distances and their approximation. *Discrete & Computational Geometry* **62**(1), 1–28 (2019). doi:[10.1007/s00454-019-00060-7](https://doi.org/10.1007/s00454-019-00060-7)
3. Bates, J.: The embedding dimension of Laplacian eigenfunction maps. *Applied and Computational Harmonic Analysis* **37**(3), 516–530 (2014). doi:[10.1016/j.acha.2014.03.002](https://doi.org/10.1016/j.acha.2014.03.002)



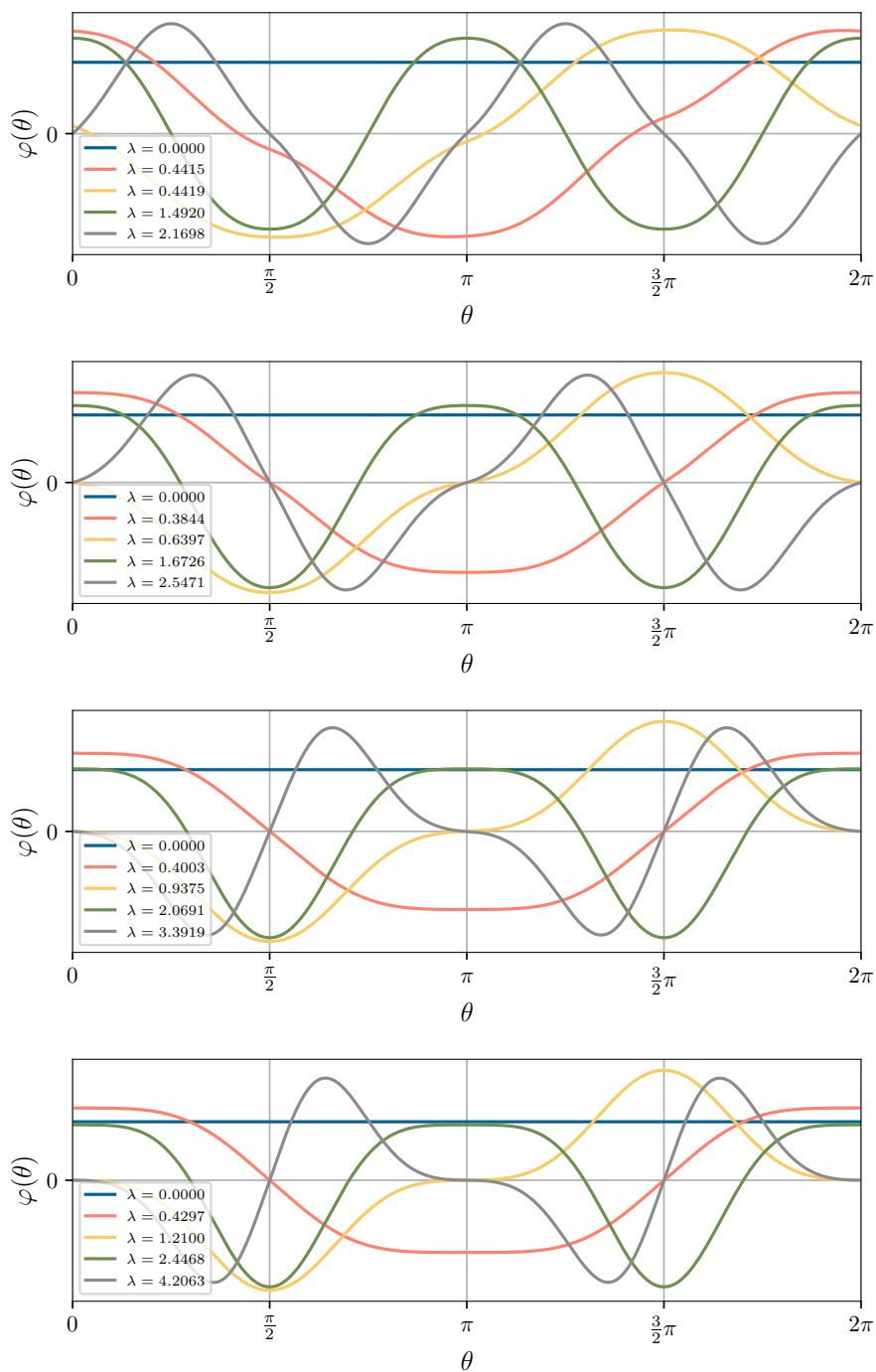


**Fig. 7** *Eigenfunctions.* The five eigenfunctions with eigenvalues smallest in magnitude for the weighted  $\ell_1$  Laplacian on the unit circle (63). These were computed numerically. In these plots, we chose  $w_2 = 1$  and all the choices  $w_1 \in \{1, 2, 4, 8\}$ , displayed from top to bottom.

4. Belkin, M., Niyogi, P.: Laplacian eigenmaps for dimensionality reduction and data representation. *Neural Computation* **15**(6), 1373–1396 (2003). doi:[10.1162/089976603321780317](https://doi.org/10.1162/089976603321780317)
5. Belkin, M., Niyogi, P.: Semi-supervised learning on Riemannian manifolds. *Machine Learning* **56**(1-3), 209–239 (2004). doi:[10.1023/B:MACH.0000033120.25363.1e](https://doi.org/10.1023/B:MACH.0000033120.25363.1e)
6. Belkin, M., Niyogi, P.: Towards a theoretical foundation for Laplacian-based manifold methods. *Journal of Computer and System Sciences* **74**(8), 1289–1308 (2008). doi:[10.1016/j.jcss.2007.08.006](https://doi.org/10.1016/j.jcss.2007.08.006)
7. Bickel, P.J., Li, B.: Local polynomial regression on unknown manifolds. *Complex Datasets and Inverse Problems*, vol. 54, pp. 177–186. Institute of Mathematical Statistics, Beachwood, Ohio, USA (2007). doi:[10.1214/074921707000000148](https://doi.org/10.1214/074921707000000148)
8. Bonnans, J.F., Shapiro, A.: Perturbation analysis of optimization problems. Springer New York, New York, NY (2000). doi:[10.1007/978-1-4612-1394-9](https://doi.org/10.1007/978-1-4612-1394-9)
9. Chazal, F., Glisse, M., Ere, C., Michel, B.: Convergence rates for persistence diagram estimation in topological data analysis. *Journal of Machine Learning Research* **16**, 3603–3635 (2015)
10. Cheng, M.Y., Wu, H.T.: Local linear regression on manifolds and its geometric interpretation. *Journal of the American Statistical Association* **108**(504), 1421–1434 (2013). doi:[10.1080/01621459.2013.827984](https://doi.org/10.1080/01621459.2013.827984)
11. Coifman, R.R., Lafon, S.: Diffusion maps. *Applied and Computational Harmonic Analysis* **21**(1), 5–30 (2006). doi:[10.1016/j.acha.2006.04.006](https://doi.org/10.1016/j.acha.2006.04.006)
12. Coifman, R.R., Lafon, S., Lee, A.B., Maggioni, M., Nadler, B., Warner, F., Zucker, S.W.: Geometric diffusions as a tool for harmonic analysis and structure definition of data: diffusion maps. *Proceedings of the National Academy of Sciences* **102**(21), 7426–7431 (2005). doi:[10.1073/pnas.0500334102](https://doi.org/10.1073/pnas.0500334102)
13. Coifman, R.R., Leeb, W.: Earth mover’s distance and equivalent metrics for spaces with hierarchical partition trees. Tech. rep., Yale University (2013)
14. Dashti, A., et al.: Retrieving functional pathways of biomolecules from single-particle snapshots. *Nature Communications* **11**(1), 4734 (2020). doi:[10.1038/s41467-020-18403-x](https://doi.org/10.1038/s41467-020-18403-x)
15. Dashti, A., et al.: Trajectories of the ribosome as a Brownian nanomachine. *Proceedings of the National Academy of Sciences* **111**(49), 17492–17497 (2014). doi:[10.1073/pnas.1419276111](https://doi.org/10.1073/pnas.1419276111)
16. Donoho, D.L., Grimes, C.: Hessian eigenmaps: locally linear embedding techniques for high-dimensional data. *Proceedings of the National Academy of Sciences* **100**(10), 5591–5596 (2003). doi:[10.1073/pnas.1031596100](https://doi.org/10.1073/pnas.1031596100)
17. Frank, J.: New opportunities created by single-particle cryo-EM: the mapping of conformational space. *Biochemistry* **57**(6), 888–888 (2018). doi:[10.1021/acs.biochem.8b00064](https://doi.org/10.1021/acs.biochem.8b00064)
18. García Trillos, N., Slepcev, D.: A variational approach to the consistency of spectral clustering. *Applied and Computational Harmonic Analysis* **45**(2), 239–281 (2018). doi:[10.1016/j.acha.2016.09.003](https://doi.org/10.1016/j.acha.2016.09.003)
19. Genovese, C.R., Perone-Pacífico, M., Verdinelli, I., Wasserman, L.: Minimax manifold estimation. *Journal of Machine Learning Research* **13**, 1263–1291 (2012)
20. Göbel, F., Blanchard, G., von Luxburg, U.: Construction of tight frames on graphs and application to denoising. *Springer Handbooks of Computational Statistics*, pp. 503–522 (2018). doi:[10.1007/978-3-319-18284-1\\_20](https://doi.org/10.1007/978-3-319-18284-1_20)
21. Goldberg, A.B., Zhu, X., Singh, A., Xu, Z., Nowak, R.: Multi-manifold semi-supervised learning. *International Conference on Artificial Intelligence and Statistics (AISTATS)*, pp. 169–176 (2009)
22. Greblicki, W., Pawlak, M.: Fourier and Hermite series estimates of regression functions. *Annals of the Institute of Statistical Mathematics* **37**(3), 443 (1985). doi:[10.1007/BF02481112](https://doi.org/10.1007/BF02481112)
23. Hein, M., Audibert, J.Y., von Luxburg, U.: From graphs to manifolds – weak and strong pointwise consistency of graph Laplacians. *International Conference on Computational Learning Theory (COLT)*, pp. 470–485 (2005). doi:[10.1007/11503415\\_32](https://doi.org/10.1007/11503415_32)
24. Hein, M., Maier, M.: Manifold denoising. *Advances in Neural Information Processing Systems (NIPS)* pp. 561–568 (2007). doi:[10.7551/mitpress/7503.003.0075](https://doi.org/10.7551/mitpress/7503.003.0075)
25. Hug, D., Weil, W.: Lectures on convex geometry, *Graduate Texts in Mathematics*, vol. 286. Springer International Publishing, Cham (2020). doi:[10.1007/978-3-030-50180-8](https://doi.org/10.1007/978-3-030-50180-8)

26. Kim, J., Rinaldo, A., Wasserman, L.: Minimax rates for estimating the dimension of a manifold. *Journal of Computational Geometry* **10**(1), 42–95 (2019). doi:[10.20382/jocg.v10i1a3](https://doi.org/10.20382/jocg.v10i1a3)
27. Kpotufe, S.:  $k$ -NN regression adapts to local intrinsic dimension. *Neural Information Processing Systems (NIPS)* pp. 1–12 (2011)
28. Lafferty, J., Wasserman, L.: Statistical analysis of semi-supervised regression. *Neural Information Processing Systems (NIPS)* (2007)
29. Landa, B., Shkolnisky, Y.: The steerable graph Laplacian and its application to filtering image datasets. *SIAM Journal on Imaging Sciences* **11**(4), 2254–2304 (2018). doi:[10.1137/18M1169394](https://doi.org/10.1137/18M1169394)
30. Lederman, R.R., Andén, J., Singer, A.: Hyper-molecules: on the representation and recovery of dynamical structures for applications in flexible macro-molecules in cryo-EM. *Inverse Problems* **36**(4), 044005 (2020). doi:[10.1088/1361-6420/ab5ede](https://doi.org/10.1088/1361-6420/ab5ede)
31. Lederman, R.R., Talmon, R.: Learning the geometry of common latent variables using alternating-diffusion. *Applied and Computational Harmonic Analysis* **44**(3), 509–536 (2018). doi:[10.1016/j.acha.2015.09.002](https://doi.org/10.1016/j.acha.2015.09.002)
32. Lee, A.B., Izbicki, R.: A spectral series approach to high-dimensional nonparametric regression. *Electronic Journal of Statistics* **10**(1), 423–463 (2016). doi:[10.1214/16-EJS1112](https://doi.org/10.1214/16-EJS1112)
33. Lee, G., Gommers, R., Waselewski, F., Wohlfahrt, K., O’Leary, A.: PyWavelets: a Python package for wavelet analysis. *Journal of Open Source Software* **4**(36), 1237 (2019). doi:[10.21105/joss.01237](https://doi.org/10.21105/joss.01237)
34. Lee, J.M.: Riemannian manifolds, *Graduate Texts in Mathematics*, vol. 176. Springer New York, New York, NY (1997). doi:[10.1007/b98852](https://doi.org/10.1007/b98852)
35. Lee, J.M.: Introduction to smooth manifolds, *Graduate Texts in Mathematics*, vol. 218. Springer New York, New York, NY (2012). doi:[10.1007/978-1-4419-9982-5](https://doi.org/10.1007/978-1-4419-9982-5)
36. Lehoucq, R.B., Sorensen, D.C., Yang, C.: ARPACK users’ guide. Society for Industrial and Applied Mathematics (1998). doi:[10.1137/1.9780898719628](https://doi.org/10.1137/1.9780898719628)
37. Li, C., Liu, H., Cai, D.: Active learning on manifolds. *Neurocomputing* **123**, 398–405 (2014). doi:[10.1016/j.neucom.2013.08.002](https://doi.org/10.1016/j.neucom.2013.08.002)
38. Lieu, L., Saito, N.: Signal ensemble classification using low-dimensional embeddings and earth mover’s distance. *Wavelets and Multiscale Analysis*, 9780817680947, pp. 227–256. Birkhäuser Boston, Boston (2011). doi:[10.1007/978-0-8176-8095-4\\_11](https://doi.org/10.1007/978-0-8176-8095-4_11)
39. von Luxburg, U., Belkin, M., Bousquet, O.: Consistency of spectral clustering. *The Annals of Statistics* **36**(2), 555–586 (2008). doi:[10.1214/009053607000000640](https://doi.org/10.1214/009053607000000640)
40. Mallat, S.: A wavelet tour of signal processing, 3rd edn. Elsevier (2009). doi:[10.1016/B978-0-12-374370-1.X0001-8](https://doi.org/10.1016/B978-0-12-374370-1.X0001-8)
41. McInnes, L., Healy, J., Saul, N., Großberger, L.: UMAP: uniform manifold approximation and projection. *Journal of Open Source Software* **3**(29), 861 (2018). doi:[10.21105/joss.00861](https://doi.org/10.21105/joss.00861)
42. Mishne, G., Talmon, R., Cohen, I., Coifman, R.R., Kluger, Y.: Data-driven tree transforms and metrics. *IEEE Transactions on Signal and Information Processing over Networks* **4**(3), 451–466 (2018). doi:[10.1109/TSIPN.2017.2743561](https://doi.org/10.1109/TSIPN.2017.2743561)
43. Mishne, G., Talmon, R., Meir, R., Schiller, J., Lavzin, M., Dubin, U., Coifman, R.R.: Hierarchical coupled-geometry analysis for neuronal structure and activity pattern discovery. *IEEE Journal of Selected Topics in Signal Processing* **10**(7), 1238–1253 (2016). doi:[10.1109/JSTSP.2016.2602061](https://doi.org/10.1109/JSTSP.2016.2602061)
44. Monera, M.G., Montesinos-Amilibia, A., Sanabria-Codeçal, E.: The Taylor expansion of the exponential map and geometric applications. *Revista de la Real Academia de Ciencias Exactas, Físicas y Naturales - Serie A: Matemáticas* **108**(2), 881–906 (2014). doi:[10.1007/s13398-013-0149-z](https://doi.org/10.1007/s13398-013-0149-z)
45. Moscovich, A., Halevi, A., Andén, J., Singer, A.: Cryo-EM reconstruction of continuous heterogeneity by Laplacian spectral volumes. *Inverse Problems* **36**(2), 024003 (2020). doi:[10.1088/1361-6420/ab4f55](https://doi.org/10.1088/1361-6420/ab4f55)
46. Moscovich, A., Jaffe, A., Nadler, B.: Minimax-optimal semi-supervised regression on unknown manifolds. *International Conference on Artificial Intelligence and Statistics (AISTATS)*, pp. 933–942. PMLR (2017)

47. Nadler, B., Lafon, S., Coifman, R.R., Kevrekidis, I.G.: Diffusion maps, spectral clustering and eigenfunctions of Fokker–Planck operators. *Neural Information Processing Systems (NIPS)*, pp. 955–962 (2005)
48. Rosasco, L., Belkin, M., De Vito, E.: On learning with integral operators. *Journal of Machine Learning Research* **11**, 905–934 (2010)
49. Ruszczynski, A.: Nonlinear optimization. Princeton University Press (2011). doi:[10.2307/j.ctvcm4hcj](https://doi.org/10.2307/j.ctvcm4hcj)
50. Shirdhonkar, S., Jacobs, D.W.: Approximate earth mover’s distance in linear time. *2008 IEEE Conference on Computer Vision and Pattern Recognition*, pp. 1–8. IEEE (2008). doi:[10.1109/CVPR.2008.4587662](https://doi.org/10.1109/CVPR.2008.4587662)
51. Singer, A.: From graph to manifold Laplacian: the convergence rate. *Applied and Computational Harmonic Analysis* **21**(1), 128–134 (2006). doi:[10.1016/j.acha.2006.03.004](https://doi.org/10.1016/j.acha.2006.03.004)
52. Singer, A., Sigworth, F.J.: Computational methods for single-particle electron cryomicroscopy. *Annual Review of Biomedical Data Science* **3**(1), 163–190 (2020). doi:[10.1146/annurev-biodatasci-021020-093826](https://doi.org/10.1146/annurev-biodatasci-021020-093826)
53. Sorzano, C.O.S., et al.: Survey of the analysis of continuous conformational variability of biological macromolecules by electron microscopy. *Acta Crystallographica Section F Structural Biology Communications* **75**(1), 19–32 (2019). doi:[10.1107/S2053230X18015108](https://doi.org/10.1107/S2053230X18015108)
54. Tenenbaum, J.B., de Silva, V., Langford, J.C.: A global geometric framework for nonlinear dimensionality reduction. *Science* **290**(5500), 2319–2323 (2000). doi:[10.1126/science.290.5500.2319](https://doi.org/10.1126/science.290.5500.2319)
55. Ting, D., Huang, L., Jordan, M.: An analysis of the convergence of graph Laplacians. *International Conference on Machine Learning (ICML)* (2010)
56. Villani, C.: Topics in optimal transportation, *Graduate Studies in Mathematics*, vol. 58. American Mathematical Society, Providence, Rhode Island (2003). doi:[10.1090/gsm/058](https://doi.org/10.1090/gsm/058)
57. Virtanen, P., et al.: SciPy 1.0: fundamental algorithms for scientific computing in Python. *Nature Methods* **17**(3), 261–272 (2020). doi:[10.1038/s41592-019-0686-2](https://doi.org/10.1038/s41592-019-0686-2)
58. Von Luxburg, U.: A tutorial on spectral clustering. *Statistics and Computing* **17**(4), 395–416 (2007). doi:[10.1007/s11222-007-9033-z](https://doi.org/10.1007/s11222-007-9033-z)
59. Wasserman, L.: Topological data analysis. *Annual Review of Statistics and Its Application* **5**(1), 501–532 (2018). doi:[10.1146/annurev-statistics-031017-100045](https://doi.org/10.1146/annurev-statistics-031017-100045)
60. Winkelbauer, A.: Moments and absolute moments of the normal distribution. *arXiv preprint arXiv:1209.4340v2* pp. 1–4 (2012)
61. Yoshida, M., Muneyuki, E., Hisabori, T.: ATP synthase – a marvellous rotary engine of the cell. *Nature Reviews Molecular Cell Biology* **2**(9), 669–677 (2001). doi:[10.1038/35089509](https://doi.org/10.1038/35089509)
62. Zelesko, N., Moscovich, A., Kileel, J., Singer, A.: Earthmover-based manifold learning for analyzing molecular conformation spaces. *IEEE International Symposium on Biomedical Imaging (ISBI)* (2020). doi:[10.1109/ISBI45749.2020.9098723](https://doi.org/10.1109/ISBI45749.2020.9098723)
63. Zhou, X., Belkin, M.: Semi-supervised learning by higher order regularization. *International Conference on Artificial Intelligence and Statistics (AISTATS)* **15**, 892–900 (2011)